hospital because of hallucinations, erythema and bladder disturbances. During this hospitalization, she suffered from dry eyes, which lead to the diagnosis of SS. Association of Hashimoto disease (autoimmune thyroiditis) was diagnosed serologically. She was transferred to our hospital for further evaluation. On admission, although her consciousness and intelligence were normal, she looked apathetic and expressionless, interpreted as severe depressive state of organic origin by a psychiatric consultant. General and neurological examinations were otherwise normal. There were no clinical symptoms of hypothyroidism. After several weeks, weakness developed suddenly and worsened to 3/5 level in the lower, and to 4/5 level in the upper extremities. The weakness was distal-dominant without fasciculation nor atrophy. The grip strength decreased to 8.5 kg in the right side and to 9 kg in the left side. Because of the weakness, she could neither stand nor walk without help. Her consciousness was alert. Extraocular movements and other cranial nerves were normal. She developed ataxia in the extremities and bladder disturbance. Sensory examination at that time revealed slight diminution in touch, pain, vibration and position sense in the lower extremities, while sensation in the area of trigeminal nerve remained unaffected. Deep tendon reflexes were severely diminished. The apathetic symptom so progressed that she could not eat enough meal, and lost her weight. Several antidepressants were tried with some improvement.

Laboratory examination revealed slight anemia, increased serum IgG (2530 mg/dl, $N<1680$ mg/dl), antinucleolar antibody (X 5120), anti-DNA antibody (X 5120, speckled pattern), SS-A antibody (X 64) and SS-B antibody (X 8). Anti-thyroglobulin and anti-microsome antibodies were positive. The biochemical examinations were otherwise normal. Schirmer test was positive, but rose bengal test was negative. The lip biopsy revealed lymphocytic infiltrates around the salivary glands. The cerebrospinal fluid contained 23 cells/mm^3 (mononuclear cells: 18; polynuclear cells: 5) and 114 mg/dl of protein, and there was no oligoclonal bands (Fig. 1). MRI of her brain showed severe cerebellar atrophy in addition to global cerebral atrophy (Fig. 2). Electrophysiological examinations showed normal central conduction time, neurogenic changes in the lower extremities by needle electromyography (EMG). Compound muscle action potential (CMAP) and sensory nerve action potential (SNAP) were nonrecordable in the right peroneal and left sural nerves, respectively. Questionable conduction block was suspected in a proximal segment of the right tibial nerve. Nerve conduction study and needle EMG were normal in the upper extremities. These findings suggested motor-dominant involvement of peripheral nerves in the lower extremities with questionable conduction block. Muscle biopsy from the left quadriceps femoris revealed scattered small-angulated fibers. The density of myelinated fibers of the sural nerve was markedly reduced to 451/mm^2 with a few myelin ovoids and clustering of small myelinated fibers. There was neither evidence of vasculitis nor of infiltration of lymphocytes. We tried corticosteroid therapy (predonisolone 60 mg/day) for several weeks, which had no influence on these neurological and psychiatric manifestations.

Fig. 1. Oligoclonal bands are not detectable in her cerebrospinal fluid.

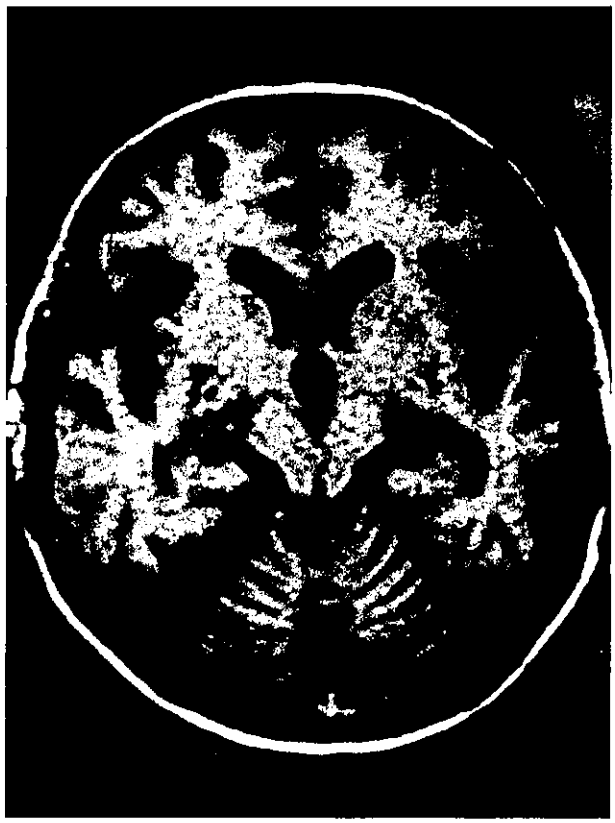

Fig. 2. T1-weighted axial MR image shows severe cerebellar atrophy in addition to severe atrophy of cerebral cortex.

3. Characterization of autoantibody

3.1. Immunohistochemistry

Brain and liver blocks were obtained from rat, mouse or bovine after fixation with 4% paraformaldehyde buffered by 0.1 M phosphate. After cryoprotection with 15% sucrose, free-floating sections were obtained on freezing microtome. Blocks were, otherwise, embedded in paraffin to obtain conventional paraffin-embedded sections. Free-floating sections or deparaffinized sections were treated with 1% hydro-

gen peroxide to block endogenous peroxydases. After incubation with 20% normal goat serum, they were incubated either with the patient's serum (1:200) or cerebrospinal fluid (1:100) for 2 days at 4 °C. The sections were then incubated with biotinylated anti-human IgG made in goat (1:200, Vector, Burlingame, CA). After reaction with avidin–biotin peroxidase complex (ABC Elite, Vector), color development was performed with diaminobenzidine enhanced by nickel as a chromogen. After counterstrained with nuclear fast red, the sections were photographed through Nomarski optics.

In deparaffinized section from the mouse brain, the patient's serum immunolabelled neuronal nuclei of the cortical neurons (Fig. 3A), neurons in the cerebellar cortex (Fig. 3B) and motor neurons in the anterior horn of the spinal cord (Fig. 3C), but not the liver tissue (Fig. 3D). Although the patient's CSF failed to label neuronal nuclei on deparaffi-

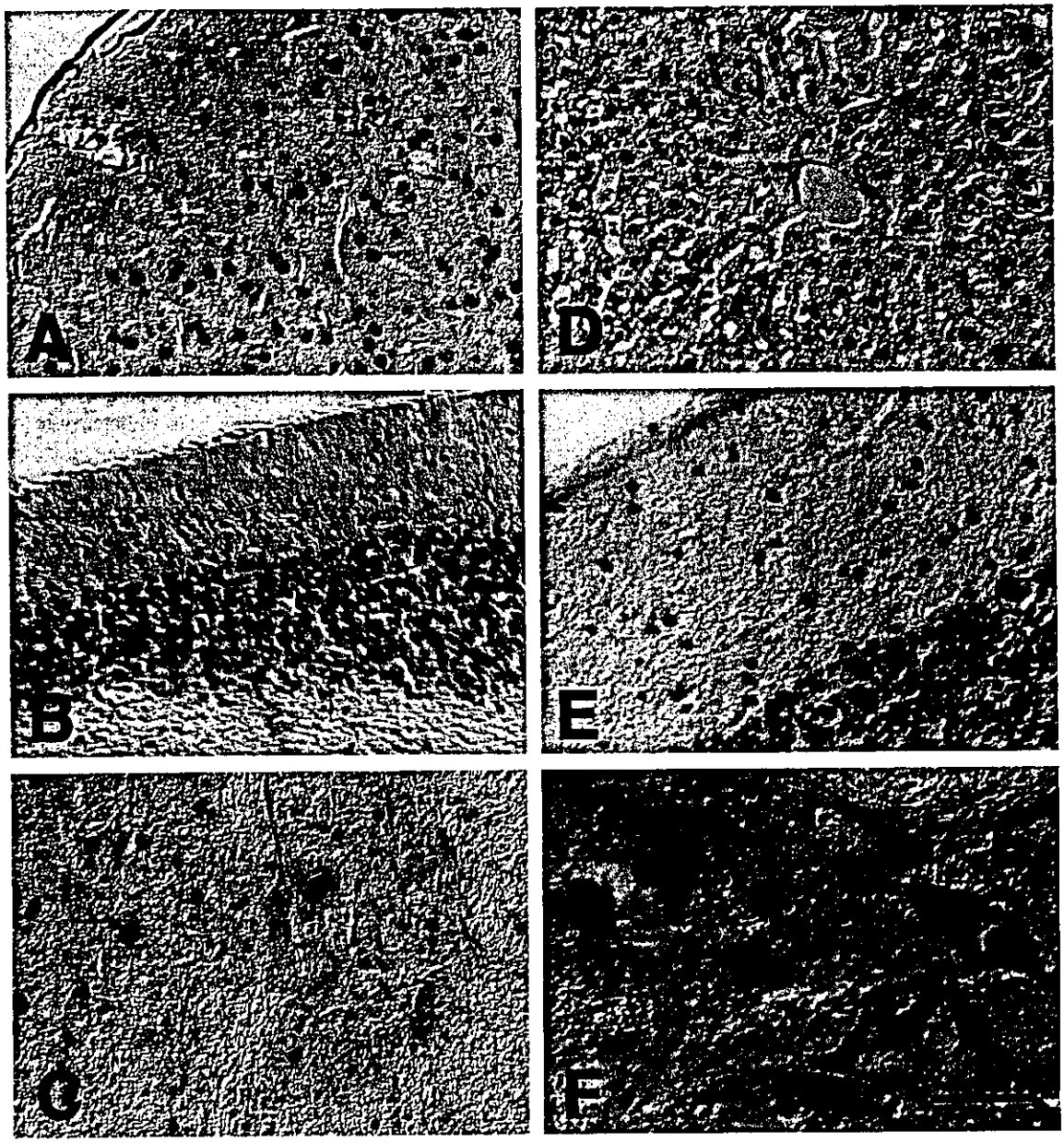

Fig. 3. Characterization of the autoantibody with immunohistochemistry. A: Mouse cerebral cortex (paraffin-embedded section) probed with the patient's serum (1:200). Nuclei of cortical neurons are immunolabelled. B: Mouse cerebellum processed and stained as A. Nuclei of cerebellar neurons are immunolabelled. C: Mouse anterior horn processed and stained as A. Nuclei of spinal motor neurons are immunolabelled. D: Mouse liver tissue processed and stained as A. No immunoreactivity is detectable. E: Rat cerebellum (free-floating section) probed with the patient's CSF (1:100) Nuclei of cerebellar neurons are immunolabelled as B. F: Bovine anterior horn (free-floating section) probed with the patient's CSF (1:100). Nuclei of spinal motor neurons are immunolabelled as C (scale bar = 50 μm, A–F).

nized sections, it immunolabelled similarly when deparaffinized sections were replaced with free-floating sections (Fig. 3E,F). Replacement of the patient's serum or CSF with control counterpart gave no immunoreactivity.

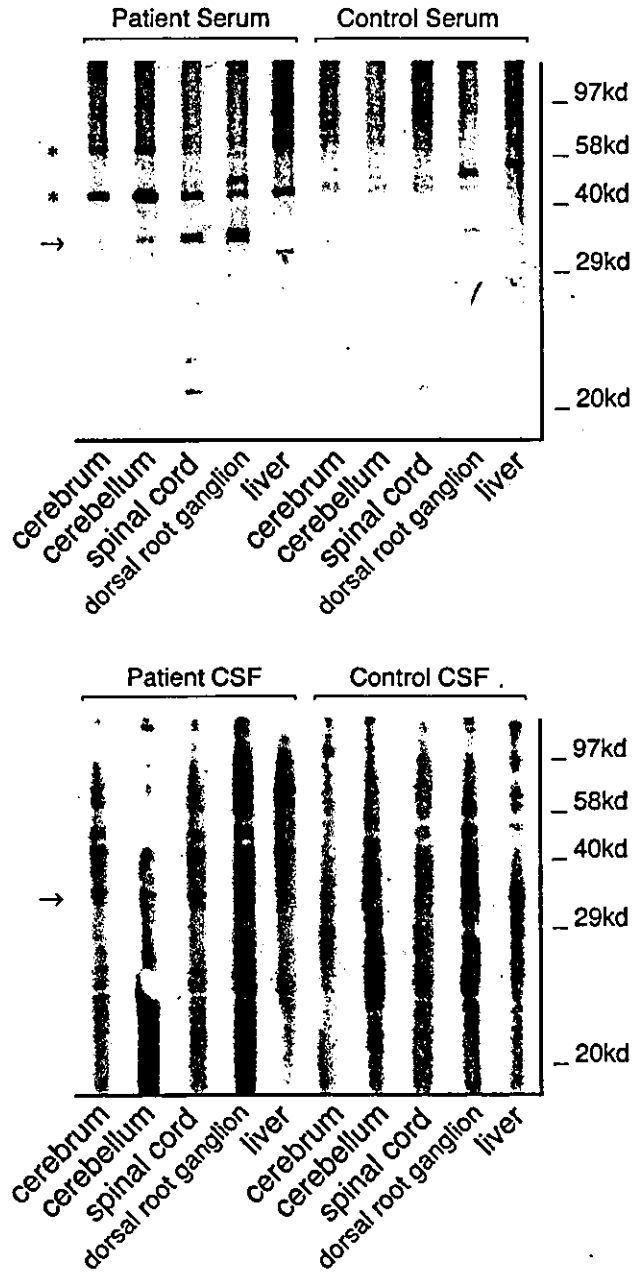

Fig. 4. Characterization of the autoantibody with Western blots. Lysate of rat cerebral cortex, cerebellum, spinal cord, dorsal root ganglion (DRG) and liver were subjected to Western blotting, probed with either serum (1:1000 dilution) (upper panel) or cerebrospinal fluid (1:125 dilution) (lower panel). The serum or cerebrospinal fluid (CSF) from a healthy subject was served as a control. The serum and CSF from the patient strongly reacted with an antigen of 34 kDa represented in the spinal cord, DRG (arrow), and with cerebellum and cerebrum, but not in the liver. There were several additional bands of different molecular weights (asterisks) when probed with the patient's serum, suggesting the presence of systemic autoantibodies, because these bands were detectable not only in the nervous tissue but also in the liver.

3.2. Western blotting

Rat cerebral cortex, cerebellum, spinal cord, dorsal root ganglion (DRG) and liver were homogenized in lysis buffer (20 mM Tris–HCl (pH 7.4), 0.1% SDS, 1% Triton X-100 and 1% sodium deoxycholate) and protein concentration of the samples was determined by the Bradford method. Samples each containing 10 μg of protein were subjected to 11% SDS-PAGE according to Laemmli. The gel was transferred onto a nitrocellulose filter. The blotted filter was blocked in TBS containing 0.1% Tween 20 (TBST) and 3% nonfat milk for 1 h at room temperature. Then it was incubated with either the serum diluted to 1:1000 (Fig. 4, upper panel), or cerebrospinal fluid (Fig. 4, lower panel) diluted to 1:125 from the patient or a control subject. The filter was washed in TBST four times and incubated in with diluted horseradish peroxidase-conjugated goat antibody or biotinylated goat antibody against human IgG(1:2000 dilution) for 1 h. After washing, immunoreactivities on the filter were detected using enhanced chemiluminescence (ECL) system or ABC systems (Vector) with 3,3-diaminobenzidine tetrahydrochloride (DAB).

The serum (Fig. 4, upper panel) and CSF (Fig. 4, lower panel) from the patient reacted with a 34-kDa antigen in the nervous system, especially in the cerebellum, spinal cord and dorsal root ganglion, which was undetectable in the liver. Several additional bands of higher molecular weights (asterisks) probed by the patient's serum were considered to represent a presence of systematic autoantibodies associated with SS, because these bands were detectable not only in the nervous tissue but also in the liver and not detectable with the patient's CSF.

4. Discussion

Various neurological manifestations have been described in SS [1,7–10]. Among them, peripheral neuropathy is the most common one, and it is observed from 10% to 28% of patients with SS [1,11,12]. Sensory nerves are preferentially affected [11,12], but the modality and distribution of neuropathy is highly variable, possibly leading to ataxic sensory neuropathy [13,14], autonomic neuropathy, distal sensory neuropathy, multiple motor neuropathy and trigeminal neuropathy [1,7–9,15]. Because the findings of needle EMG and nerve conduction of this patient are compatible with neurogenic changes, the sudden-onset motor weakness which accompanied markedly diminished reflexes and slight sensory disturbance was diagnosed as motor neuropathy and/or motor neuronopathy in this patient. Although involvement of motor nerves in SS has been reported only rarely [1,15–17], motor-dominant weakness of peripheral nerve origin in SS as observed in our case has not yet been described. The underlying mechanisms of peripheral neuropathy in SS are also highly heterogeneous, for example, vasculitis [1], secondary ischemic changes [9,18], necrotiz-

ing asteritis [19], inflammation without vasculitis [11] and necrotizing dorsal root ganglionitis [11,13]. Motor-dominant neuropathy in the lower extremities as seen in our patient, however, is hard to be explained by these mechanisms. Moreover, lack of specific findings in the sural nerve biopsy specimen failed to specify neither vasculitis nor other mechanisms mentioned above.

Involvement of the central nervous system in SS is far more variable, presenting with aseptic meningitis [20], epilepsy [2,21], symptoms mimicking multiple sclerosis [4,22], or psychiatric symptoms such as psychosis and depressive state [3,8,23,24]. Lack of lateralized symptoms and the absence of local lesions in our patient, however, are not compatible with localized pathology such as vasculitis [9,15,16,19] or demyelinating foci [4,22]. Several autoantibodies against neural tissues have been reported in SS as a candidate to explain this kind of non-focal neurological manifestations of SS. Reported examples are very rare and may possibly include one that reacts with cerebellar Purkinje cells [4] as anti-Hu antibody does and another against DRG cells in a patient with severe sensory neuropathy associated with SS [6], both of which, however, await further characterization with more precision. In our patient, an affinity of this autoantibody to spinal motor neurons, which has not been reported so far, may correspond to her motor symptoms. In addition, our patient developed ataxia and depression, both of which are rare complications of SS. Although ataxic symptoms could be caused by peripheral lesions, scarcity of involvement in deep, position and vibration sensation in her lower extremities are hard to explain the ataxia [12–14,25]. Cerebellar atrophy shown by brain MRI in the presence of this autoantibody, which reacted with a 34-kDa antigen also present in cerebellar Purkinje cells, suggests cerebellar origin of her ataxia. Because the target antigen recognized by this autoantibody is present also in the cerebellar Purkinje cells, it is likely that this cerebellar ataxia and atrophy may be mediated by this autoantibody. Although the epitope detected by this autoantibody remains to be identified, these restricted neurons containing its 34-kDa target antigen correspond well to neurological manifestations of this patient, which suggests pathogenic role of this autoantibody. Moreover, its failure to react with the extraneuronal tissue indicates its preferential affinity to the nervous tissue. While it remains to be proved whether this autoantibody is produced in the nervous system, it is likely that the presence of this antineuronal antibody in the cerebrospinal fluid may have facilitated the development of these neurological manifestations. Because of administration of corticosteroids, which usually exhibits anti-inflammatory effects not directly related to the production of antibodies, the lack of clinical improvement after its administration may be explained if this autoantibody had some pathogenic significance.

In summary, some of the autoantibodies, found occasionally in SS patients, react with epitopes exclusively represented in neuronal tissue, as we demonstrated in this patient. In the absence of other documented pathological processes in this patient, such as vasculitis or demyelination, this preferential affinity of this autoantibody to nervous tissue and its presence in the cerebrospinal fluid may be one of the most plausible candidates to explain the neurological manifestations of this patient. Although identification of target antigens recognized by this autoantibody is of prime importance, removal or inactivation of this antibody may provide a rational clinical strategy to treat a group of SS patients with neurological manifestations linked to an autoantibody.

References

[1] Kaplan JG, Rosenberg R, Reinitz E, et al. Invited review: peripheral neuropathy in Sjögren syndrome. Muscle Nerve 1990;13:570–9.

[2] Alexander GE, Provost TT, Stevens MB, et al. Sjögren syndrome: central nervous system manifestations. Neurology 1981;31:1391–6.

[3] Malinow KL, Molina R, Gordon B, et al. Neuropsychiatric dysfunction in primary Sjögren's syndrome. Ann Intern Med 1985;103:344–50.

[4] Alexander EL, Malinow K, Lejewski JE, et al. Primary Sjögren's syndrome with central nervous system disease mimicking multiple sclerosis. Ann Intern Med 1986;104:323–30.

[5] Alexander EL, Lijewski JE, Jerdan MS, et al. Evidence of an immunopathogenic basis for central nervous system disease in primary Sjögren's syndrome. Arthritis Rheum 1986;29:1223–31.

[6] Terao Y, Sakai K, Kato S, et al. Antineuronal antibody in Sjögren's syndrome masquerading as paraneoplastic cerebellar degeneration. Lancet 1994;343:790.

[7] Kaltreider HB, Talal N. The neuropathy of Sjögren's syndrome. Trigeminal nerve involvement. Ann Intern Med 1969;70:751–62.

[8] Hietaharju A, Yli-Kerttula U, Hakkinen V, et al. Nervous system manifestations in Sjögren's syndrome. Acta Neurol Scand 1990;81:144–52.

[9] Peyronnard JM, Charron L, Beaudet F, et al. Vasculitic neuropathy in rheumatoid disease and Sjögren syndrome. Neurology 1982;32:839–45.

[10] Sorajja P, Poirier MK, Bundrick JB, et al. Autonomic failure and proximal skeletal myopathy in a patient with primary Sjögren syndrome. Mayo Clin Proc 1999;74:695–7.

[11] Graus F, Pou A, Kanterewicz E, et al. Sensory neuronopathy and Sjögren's syndrome: clinical and immunologic study of two patients. Neurology 1988;38:1637–9.

[12] Laloux P, Brucher JM, Guerit JM, et al. Subacute sensory neuronopathy associated with Sjögren's sicca syndrome. J Neurol 1988;235:352–4.

[13] Malinow K, Yannakakis GD, Glusman SM, et al. Subacute sensory neuronopathy secondary to dorsal root ganglionitis in primary Sjögren's syndrome. Ann Neurol 1986;20:535–7.

[14] Griffin JW, Cornblath DR, Alexander E, et al. Ataxic sensory neuropathy and dorsal root ganglionitis associated with Sjögren's syndrome. Ann Neurol 1990;27:304–15.

[15] Mellgren SI, Conn DL, Stevens JC, et al. Peripheral neuropathy in primary Sjögren's syndrome. Neurology 1989;39:390–4.

[16] Alexander EL, Provost TT, Stevens MB, et al. Neurologic complications of primary Sjögren's syndrome. Medicine 1982;61:247–57.

[17] Inoue A, Koh CS, Tsukuda N, et al. Peripheral neuropathy associated with Sjögren's syndrome: pathologic and immunologic study of two patients. Jpn J Med 1991;30:452–7.

[18] Uchihara T, Yoshida S, Tsukagoshi H. Bilateral facial paresis with Sjögren's syndrome. J Neurol 1989;236:186.

[19] Alexander EL, Craft C, Dorsch C, et al. Necrotizing arteritis and

spinal subarachnoid hemorrhage in Sjögren syndrome. Ann Neurol 1982;11:632–5.
[20] Alexander ÉL, Alexander GE. Aseptic meningoencephalitis in primary Sjögren's syndrome. Neurology 1983;33:593–8.
[21] Bansal SK, Sawhney IM, Chopra JS. Epilepsia partialis continua in Sjögren's syndrome. Epilepsia 1987;28:362–3.
[22] Miro J, Pena-Sagredo JL, Berciano J, et al. Prevalence of primary Sjögren's syndrome in patients with multiple sclerosis. Ann Neurol 1990;27:582–4.
[23] Tarter RE, Hays AL, Carra J, et al. Sjögren's syndrome. Its contribution to neuropsychiatric syndrome in patients with primary biliary cirrhosis. Dig Dis Sci 1989;34:9–12.
[24] Spezialetti R, Bluestein HG, Peter JB, et al. Neuropsychiatric disease in Sjögren's syndrome: anti-ribosomal P and anti-neuronal antibodies. Am J Med 1993;95:153–60.
[25] Satake M, Yoshimura T, Iwaki T, et al. Anti-dorsal root ganglion neuron antibody in a case of dorsal root ganglionitis associated with Sjögren's syndrome. J Neurol Sci 1995;132:122–5.

GLIA 45:180–187 (2004)

Microglial Tau Undergoes Phosphorylation-Independent Modification After Ischemia

TOSHIKI UCHIHARA,[1]* AYAKO NAKAMURA,[1] TETSUAKI ARAI,[2] KENJI IKEDA,[2] AND KUNIAKI TSUCHIYA[3]

[1]*Department of Neuropathology, Tokyo Metropolitan Institute for Neuroscience, Tokyo, Japan*
[2]*Department of Psychogeriatrics, Tokyo Institute of Psychiatry, Tokyo, Japan*
[3]*Department of Laboratory Medicine and Pathology, Tokyo Metropolitan Matsuzawa Hospital, Tokyo, Japan*

KEY WORDS conformation; tau2; epitope; detergent; immunohistochemistry

ABSTRACT Tau2 is a phosphorylation-independent antibody that immunolabels neurofibrillary tangles (NFTs) of Alzheimer type and microglia around ischemic foci on formalin-fixed, paraffin-embedded sections. We found that copresence of polyethyleneglycol-*p*-isooctylphenyl ether (Triton X-100; TX) with tau2 abolished its immunoreactivity (IR) in these microglia but not its IR on NFTs. Tau2-immunoreactive bands, exclusively retrieved in Tris-soluble fraction of brain homogenates from ischemic foci, normal human and bovine brains, were of similar electrophoretic mobility, indicating that tau2 IR in these microglia is unrelated to hyperphosphorylation of tau. These tau2-immunoreactive bands except those from bovine brain were abolished in the copresence of TX. This was not due to washing out of tau, because similar immunoreactive bands were detectable with another antitau antibody even under a higher concentration of TX and because washing after TX exposure restored similar tau2 IR both on immunohistochemisty and immunoblot. These findings are explained if tau, modified after ischemia, undergoes a reversible conformational change on TX exposure. Because conformation at Ser101 of bovine tau is crucial for its affinity to tau2, this Ser-like conformation mimicked by its human counterpart Pro may represent pathological modification of tau shared by microglia around ischemic foci and NFTs. Relative resistance of tau2 epitope in NFTs to TX exposure suggests that tau woven into NFTs confers additional stability to this pathological modification on tau2 epitope. Susceptibility of tau2 epitope to TX, seen in these microglia, is shared with glial cytoplasmic inclusions and will show its conformational state to be different from that in NFTs.

INTRODUCTION

Ischemic insults to the brain tissue trigger a variety of cascades leading to cell death and glial proliferation. Although these are usually acute reactions, molecules participating in these processes and their changes are partly shared with chronic neurodegenerative disorders. One example is the appearance of tau-like immunoreactivity (IR) in glial and in neuronal cells. Unmodified tau proteins in normal brain tissue, which are easily detectable with immunoblot, are hardly visualized with immunohistochemistry on fixed brain tissue. It is therefore speculated that some modification of tau, for example, pathological phosphorylation as seen in degenerative tauopathies (Lee et al., 2001), is a prerequisite for immunohistochemical visualization of tau on fixed brain tissue (Pollock and Wood, 1988; Matsuo et al., 1994), but its precise molecular mechanism remains to be clarified. It has been reported that a vari-

*Correspondence to: Dr. Toshiki Uchihara, Department of Neuropathology, Tokyo Metropolitan Institute for Neuroscience, 2-6 Musashi-dai, Fuchu, Tokyo 183-8526, Japan. E-mail: uchihara@tmin.ac.jp

Received 12 June 2003; Accepted 8 August 2003

DOI 10.1002/glia.10318

Published online 20 October 2003 in Wiley InterScience (www.interscience.wiley.com).

TABLE 1. Summary of Clinical Data

Number of case[a]	Age at death (years)	Sex	Time[b]	Diagnosis
9 (3)	49–89	3 M/6 F	8 days to 11 months	Infarction
6 (4)	66–84	2 M/4 F	4–16 years	AD
8 (4)	53–90	5 M/3 F		Normal

[a]Number of cases used for immunoblot in parentheses.
[b]Time from onset of ischemic attack or AD to death.

ety of cells are immunostained by limited antitau antibodies after brain ischemia, whereas the epitopes visualized and cell types vary according to different experimental conditions (Dewar et al., 1993; Geddes et al., 1994; Dewar and Dawson, 1995; Odawara et al., 1995; Uchihara et al., 1995, 2000; Irving et al., 1996, 1997). Moreover, it remains to be settled whether the appearance of tau-immunopositive glial cells in human brain after ischemic insult is related to pathological hyperphosphorylation of tau. We therefore attempted to characterize these tau-positive glial cells in human brains with ischemia by using immunohistochemistry and immunoblotting with a panel of antitau antibodies and compared the findings with those obtained on brains with Alzheimer's disease (AD). Immunohistochemical screening with a panel of antitau antibodies clarified that microglial cells around ischemic foci, irrespective of the interval after the relevant ischemic attack, were selectively immunopositive for tau2, one of the phosphorylation-independent antibodies raised against bovine tau (Papasozomenos and Binder, 1987), as reported by different groups (Papasozomenos and Binder, 1987; Odawara et al., 1995; Uchihara et al., 2000). We later became aware that this tau2 IR in microglia was abolished when the sections were incubated with tau2 diluted in a buffer containing polyoxylethyleneglycol-*p*-isooctylphenyl ether (Triton X-100; TX) as we reported on glial cytoplasmic inclusions (GCIs) seen in multiple-system atrophy (Shibuya et al., 2003). It is then possible that modification of tau in glial cells, possibly shared between microglia around ischemic focus and GCIs, may be different from neurofibrillary tangles (NFTs) in neurons. In the present study, we examined this tau2 IR and possible influences of TX. Influence of TX on tau2 IR may represent its possible conformational change, characteristic of glial cells in brain ischemia.

MATERIALS AND METHODS

Autopsied brains from nine patients with cerebral infarction, six patients with AD, and eight patients without neurological disorders were enrolled in this study as shown in Table 1. The time from the onset of the disease to death was determined from the clinical records.

Immunohistochemistry

Formalin-fixed, paraffin-embedded blocks including both the area of ischemic necrosis and the surrounding nonnecrotic area were obtained. Blocks from the temporal lobe were sampled from AD brains. Ten-micron-thick sections were deparaffinized and treated with 1% hydrogen peroxide for 15 min. After being incubated with phosphate-buffered saline (PBS) containing 5% normal horse serum, the sections were incubated with one of the following antibodies: tau2 (1:500; Sigma, St. Louis, MO) (Papasozomenos and Binder, 1987), anti-human tau (pool2; 1;10,000; a generous gift from Professor Y. Ihara, University of Tokyo) (Endoh et al., 1993), Alz-50 (1:200; a generous gift from Professor P. Davies, Albert Einstein University) (Wolozin et al., 1986), or antipaired helical filaments (anti-PHF; AT8; 1:10,000; Innogenetics, Zwijndrecht, Belgium) (Mercken et al., 1992) diluted in PBS containing different concentrations of TX at room temperature for 1 h. The sections were then incubated with a biotinylated secondary antibody (1:500; Vector, Burlingame, CA) for 1 h at room temperature. They were then incubated with avidin-biotin-peroxidase complex (1:500; ABC Elite, Vector) and the labeling was visualized with diaminobenzidine and nickel ammonium chloride as a chromogen.

Disappearance of tau2 IR on exposure to TX and its reappearance were assessed in two ways on histological sections. Deparaffinized sections from ischemic foci, treated with 1% hydrogen peroxide, were incubated with 0.1% TX-PBS for 1 h before immunohistochemistry and subsequently washed in PBS for 1–3 h. They were then incubated with tau2 in the absence of TX and similarly processed as described above. Separate sections were incubated with tau2 either in the absence [TX(−)] or in the presence of TX in parallel. Otherwise, deparaffinized sections, treated with 1% hydrogen peroxide, were first incubated with tau2 in the absence of TX and then exposed to different concentrations of TX (0–0.3%) for 3 h. Subsequent steps were performed similarly in the absence of TX to visualize the remaining tau2.

Fractionation of Frozen Brains

Affected areas of cerebral cortices were sampled from frozen brains of cerebral infarction or of AD. Cerebral cortices from normal bovine or autopsied human brains without neurological disorders were also sampled. These samples were homogenized in serial solutions with increasing solubilization capacity as indicated below, which made it possible to investigate an entire spectrum of tau from normal to a highly aggregated form (Endoh et al., 1993; Arai et al., 2001). In order to minimize nonspecific proteolysis of tau, buffers were routinely prepared to contain 0.5 mM di-isopropyl fluorophosphate, 0.5 mM phenylmethylsulfonyl fluoride, 1 μg/ml antipain, 0.1 μg/ml pepstatin, and 1 μg/ml

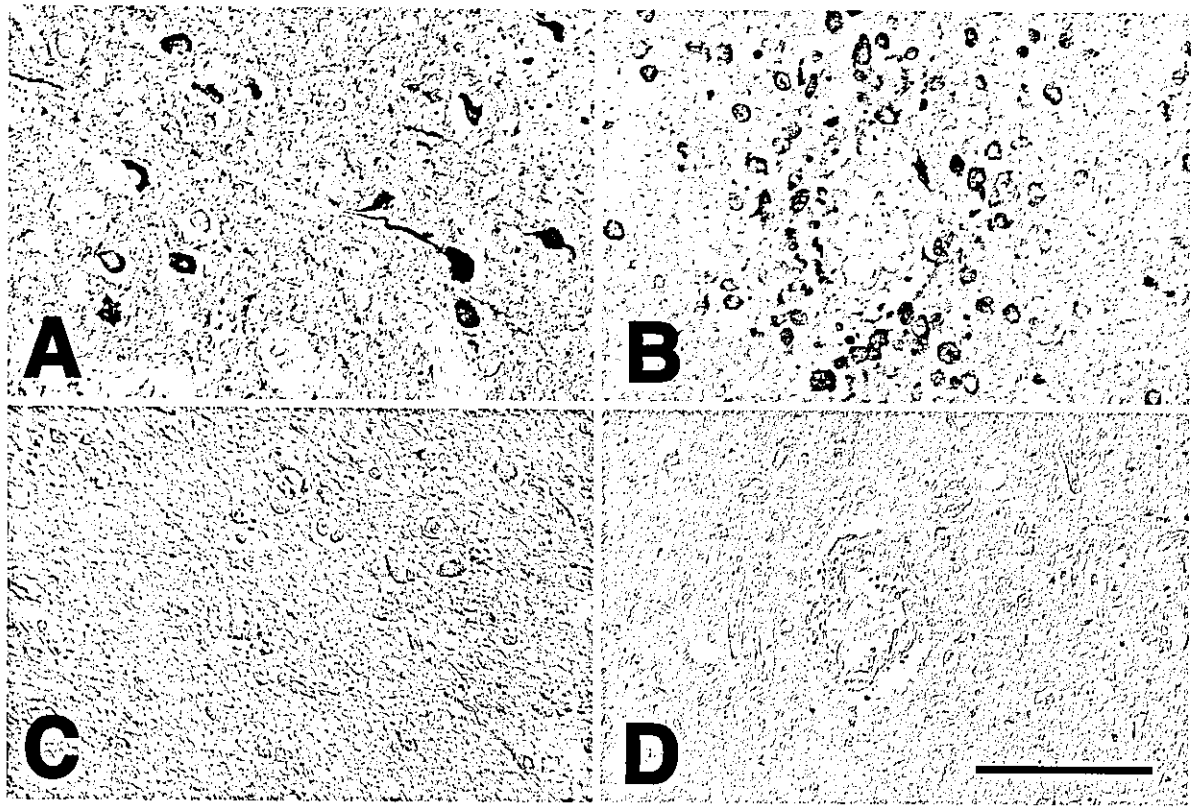

Fig. 1. Tau2 immunolabeled neurofibrillary tangles (**A**) and microglial cells around an ischemic focus (**B**). Tau2 immunolabeling was abolished on incubating the sections (**C** and **D**) with tau2 diluted in buffer containing the specific blocking peptide (bar = 50 μm).

leupeptin. Approximately 1 g of brain tissue was homogenized and fractionated sequentially with 2 ml of Tris-buffered saline (TS; 50 mM Tris, pH 7.6, 150 mM NaCl), with the same volume of 1% sarkosyl/TS, 2% sodium dodecyl sulfate (SDS)/TS, and then formic acid (> 99%). Soluble and insoluble fractions were separated by centrifugation (200,000 *g* for 20 min) at 4°C for TS and sarkosyl/TS or at room temperature for SDS/TS and formic acid. PHF fraction was prepared from AD brains as described previously (Greenberg and Davies, 1990; Goedert et al., 1992).

Immunoblotting

The supernatant of each fraction (10 μl for each lane) was treated with SDS sample buffer, boiled for 5 min, then subjected to 10% SDS-PAGE. Proteins in the gel were electronically transblotted onto a nitrocellulose filter (BioRad, Hercules, CA). The filters were incubated with Tris-buffered saline (TBS; 20 mM Tris, pH 7.6, NaCl 150 mM)/5% nonfat milk. They were then incubated for 1 h at room temperature with tau2 (1:2,000) diluted in TBS/5% nonfat milk containing different concentrations of TX. After being washed for 10 min three times, the filters were incubated with HRP-tagged antimouse IgG (1:4,000; Kirkegaard and Perry, Gaithersburg, MD) for 1 h and tau2-immunoreactive bands were visualized with electrochemiluminescence (ECL; Amersham, U.K.). Peroxidase activity remaining on the filter was then inactivated by incubating it for 20 min with 2% hydrogen peroxide in TBS. After being blocked with TBS/5% nonfat milk, the filter was reprobed with an anti-human tau antibody (pool2, 1:100,000) diluted in TBS containing 0.1% TX for 24 h. The filter was incubated with HRP-tagged antirabbit IgG (1:5,000; Pierce, Rockford, IL) for 2 h and subjected to ECL. Disappearance of tau2 IR on exposure to TX and its reappearance were assessed also on immunoblot. The blotted filters were incubated with 0.06% TX-TBS for 1 h before immunodetection and subsequently washed in TBS for 3 h. They were then incubated with tau2 in the absence of TX and were processed similarly to the process described above. Separate filters were incubated with tau2 either in the absence or in the presence of TX in parallel.

RESULTS

Tau2 immunolabeled NFTs of AD brains (Fig. 1A), as well as microglial cells around ischemic foci (Fig. 1B) in the absence of TX. Other antitau antibodies (antihuman tau pool2; 1:10,000) (Endoh et al., 1993), Alz-50

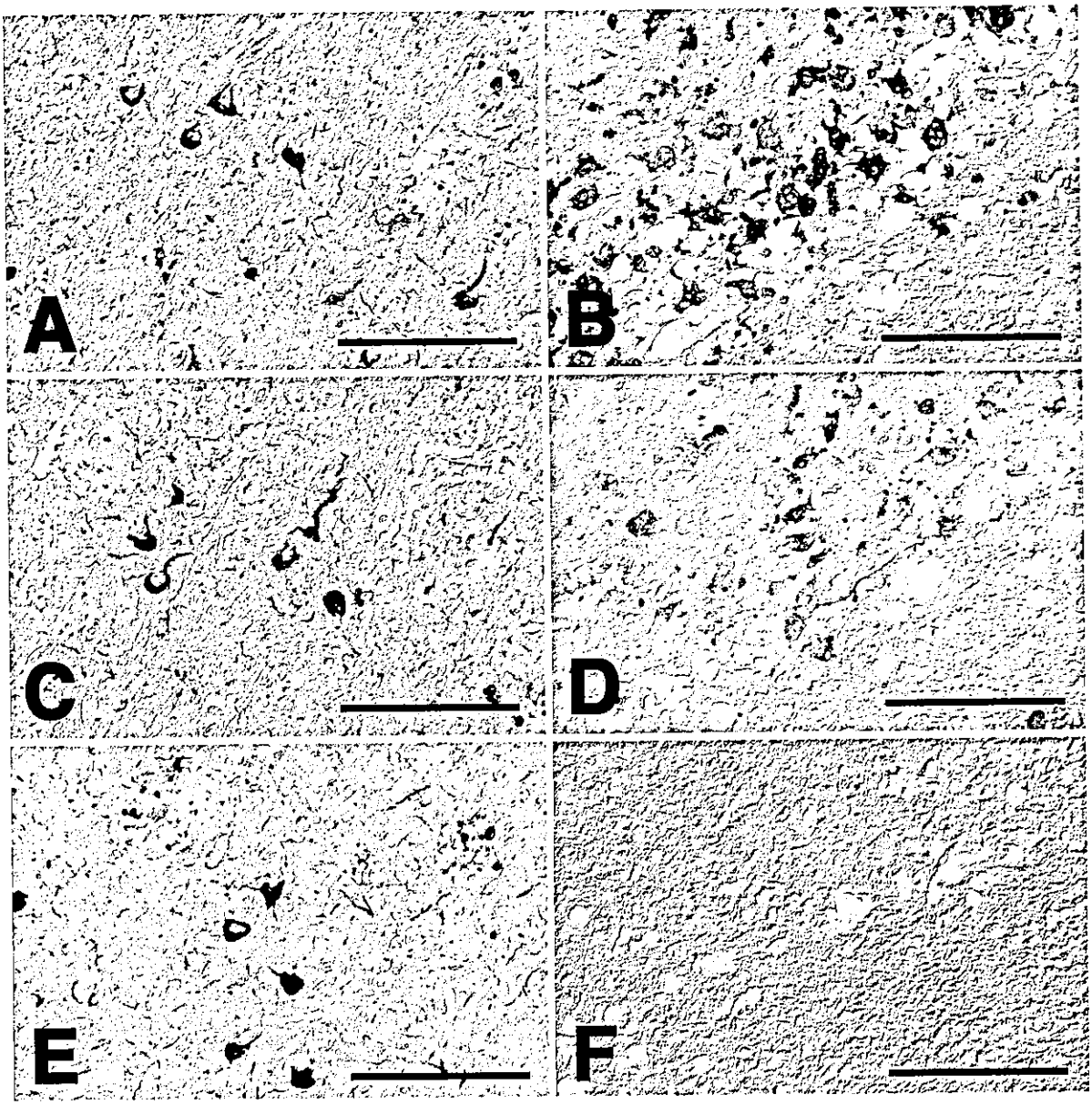

Fig. 2. Influence of Triton X-100 on tau2 immunolabeling. Sections from AD brain (**A**, **C**, and **E**; bars = 100 μm) and around ischemic focus (**B**, **D**, and **F**; bars = 50 μm) were immunolabeled with tau2 diluted in PBS containing 0% (A and B), 0.01% (C and D), or 0.03% (E and F) TX. Tau2 immunolabeling on microglial cells (B) decreased with increasing concentrations of TX (D and F), whereas that on NFTs remained stable (C and E).

(1:200) (Wolozin et al., 1986), and anti-PHF tau (AT8; 1:10,000) (Mercken et al., 1992) immunolabeled NFTs but failed to immunolabel these microglial cells around ischemic foci and normal bovine brain even in the absence of TX (data not shown). This tau2 IR was completely abolished (Fig. 1C and D) when the histological sections were incubated with tau2 and a synthetic peptide (AGIGDTS*NLEDQAA), which corresponded to the tau2 epitope of bovine tau (Watanabe et al., 1992). When tau2 was diluted with PBS containing TX, a reduction in tau2 IR in these microglial cells was apparent and it was dependent on the concentration of TX (Fig. 2B, D, and F), but this TX-dependent reduction in tau2 IR was not apparent on NFTs with the concentration of TX up to 0.06% (Fig. 2A, C, and E). Pretreatment with TX (0.1% for 1 h) abolished tau2 IR (Fig. 3B). But subsequent washing with PBS not containing TX for up to 3 h restored this tau2 IR on these microglial cells (Fig. 3C and D). Exposure of sections to TX after incubation with tau2 (in the absence of TX) reduced its IR with increasing concentrations of TX (Fig. 4).

Tau2-immunoreactive bands were detected in the TS-soluble fraction of normal control brains and of ischemic focus (Fig. 5, column a). In AD brains, they were retrieved in the SDS-soluble fraction (Fig. 5, column c) and PHF fraction (Fig. 5, column e) and were of

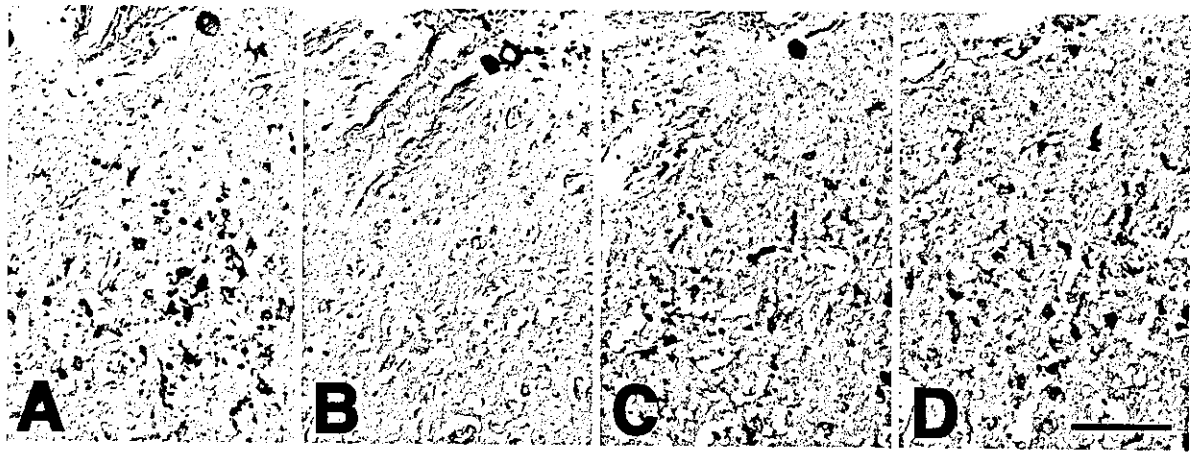

Fig. 3. Disappearance of tau2 immunolabeling on exposure to TX and its restoration after washing. Serial sections around an ischemic focus (A–D; bar = 50 μm) were stained with tau2 in the absence (A) or presence (B) of 0.1% TX. Reduced tau2 immunolabeling on exposure to TX (0.1% for 1 h; B) was restored progressively after washing for 1 (C) and 3 h (D) prior to immunodetection.

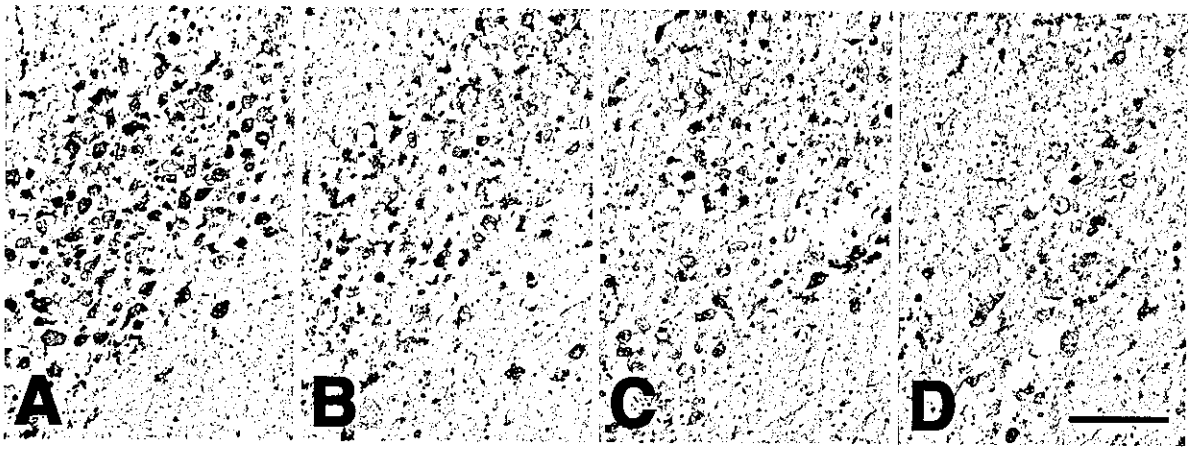

Fig. 4. Dissociation of tau2 binding on exposure to TX. Serial sections around an ischemic focus (A–D; bar = 50 μm) were first incubated with tau2 in the absence of TX. They were then washed with PBS containing different concentrations of TX (A, 0%; B, 0.003%; C, 0.03%; D, 0.3%) for 3 h and the remaining tau2 was visualized in the absence of TX. Bound tau2 (A) dissociated on exposure to TX, which is dependent on the concentration of TX (B–D).

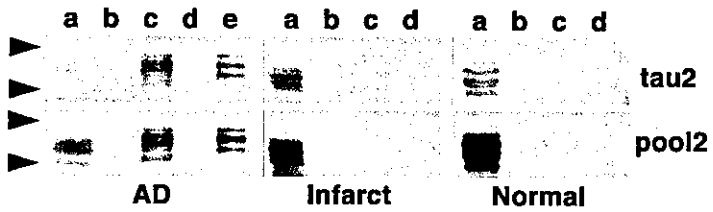

Fig. 5. Fractions serially separated (a, Tris-soluble; b, sarkosyl-soluble; c, SDS-soluble; d, formic acid-extracted; e, PHF fractions) from brain homogenate (Infarct: cerebral infarction; Normal: normal control) were subjected to 10% SDS-PAGE and were probed with tau2 (upper line). The same blotted filters were reprobed with pool2 (lower line). Upper arrowhead, 68 kDa; lower arrowhead, 50 kDa. Tau2-immunoreactive bands were similarly probed with pool2. Tau-immunoreactive bands from brain with cerebral infarction were retrieved in TS-soluble fraction and exhibited an electrophoretic mobility similar to those from normal brain. SDS-soluble fraction (c) from AD brain contained tau species with a decreased electrophoretic mobility equivalent to PHF tau (e).

higher molecular weight than those observed in normal control brain and in ischemic focus. Sarkosyl-soluble (Fig. 5, column c) and formic acid-extracted (Fig. 5, column d) fractions did not exhibit tau2-immunoreactive bands. These tau2-immunoreactive bands were similarly visualized when the same filters were subsequently probed with another antihuman tau antibody (pool2; Fig. 5, lower line). These tau2-immunoreactive bands were absorbed by coincubation with the same synthetic peptide (AGIGDTS*NLEDQAA) as we demonstrated on histological sections (data not shown). Tau2 IR in the TS fraction from bovine brain was so

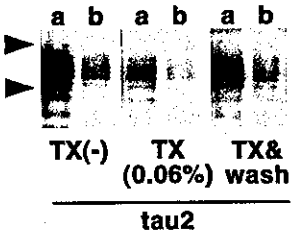

Fig. 6. Tris-soluble fractions from bovine brain diluted to 1:300 (a) or 1:1,000 (b) were subjected to 10% SDS-PAGE and probed with tau2 in the absence [TX(−)] or the presence [TX(0.06%)] of TX. Tau2-immunoreactive bands retained their intensity even in the presence of TX. Their intensity, partially decreased on exposure to TX, was restored to normal after washing (TX&wash). Upper arrowhead, 68 kDa; lower arrowhead, 50 kDa.

intense that this fraction should be diluted to 1:300 (Fig. 6, column a) to 1:1,000 (Fig. 6, column b) to give tau2 IR equivalent to those observed with fractions originating in human brains [Fig. 6, TX(−)] (Watanabe et al., 1992). When the blotted filter was incubated with tau2 in TBS containing more than 0.06% of TX [Fig. 7, TX(0.06%)], these tau2-immunoreactive bands in any fraction from human brains [Fig. 7, TX(−), column a: SDS-soluble fraction from AD; column b: PHF fraction from AD; column c: Tris-soluble fraction from infarction; and column d: Tris-soluble fraction from normal control] were not detectable, regardless of the disease, while those from bovine brain remained tau2-immunoreactive even in the presence of 0.06% TX [Fig. 6, TX(0.06%)]. Extensive washing with TBS (for 3 h) after pretreatment with TX (0.06% for 1 h) restored this tau2 IR on these bands (Figs. 6 and 7, TX&wash). Reprobing the same filter, which failed to exhibit tau-2-immunoreactive bands in the presence of TX [Fig. 7, TX(0.06%)], with another antihuman tau antibody (pool2) visualized similar tau-positive bands, even in the presence of 0.1% TX [Fig. 7, TX(0.1%)].

DISCUSSION

It has been reported previously that brain ischemia is associated with the appearance of tau2-positive microglial cells (Odawara et al., 1995; Uchihara et al., 2000) in human autopsied samples. Although both microglial cells around ischemic foci and NFTs were similarly immunolabeled with tau2 on fixed histological sections, this study distinguished the two conditions by demonstrating that homogenate from ischemic foci contained tau2-immunoreactive bands with an electrophoretic mobility indistinguishable from that of normal tau; that coincubation of tau2 with TX abolished the tau2 IR on microglial cells in a reversible fashion, whereas tau2 IR on NFTs was less affected; and that other antitau antibodies immunolabeled NFTs but not these microglial cells. These characteristics of microglial cells around ischemic foci are identical to what we demonstrated on GCIs (Shibuya et al., 2003).

Immunoblot of the brain homogenates demonstrated that tau2-immunoreactive bands from ischemic foci were detected exclusively in the TS fraction. Because it was the only fraction that contained tau-immunoreactive bands (Fig. 5, infarct, column a), tau2 IR observed in microglial cells around ischemic foci corresponded to these tau2-immunoreactive bands, even though they were indistinguishable from those observed in normal brain tissue (Fig. 5, normal, column a). The specificity of this tau2 immunolabeling was established by the reduction in tau2 IR when the sections or immunoblotted filters were incubated with tau2 and the peptide corresponding to its putative epitope. Because histological sections from normal bovine brain, even containing tau with an extremely high affinity [nearly 1,000-fold; Fig. 6, TX(−), column b] for tau2 on immunoblot, failed to exhibit apparent immunohistochemical labeling with tau2, immunohistochemical visualization of tau2 epitope is dependent on some pathological modifications of tau proteins (Pollock and Wood, 1988; Papasozomenos and Su, 1991; Matsuo et al., 1994) rather than on their quantity. Indeed, the relative intensity of tau-immunoreactive bands, detected either with tau2 or pool2, was similar in the TS fraction from ischemic foci to that from normal brain (Fig. 5). Experimental data on cultured cells or animal models have demonstrated that tau proteins are transiently dephosphorylated but never hyperphosphorylated during ischemia and reperfusion or similar experimental conditions (Dewar and Dawson, 1995; Shackelford and Nelson, 1996; Burkhart et al., 1998; Shackelford and Yeh, 1998). It is therefore probable that tau protein in ischemic foci undergoes some pathological modifications to be visualized on immunohistochemistry, although these modifications are not necessarily related to phosphorylation and are indistinguishable from unmodified human tau protein on routine immunoblot, as we demonstrated on GCIs (Shibuya et al., 2003).

It is interesting that the two antibodies, Alz50 and tau2, both dependent on conformation of tau (Carmel et al., 1996), immunolabel tau around the ischemic area. Although both antibodies recognize PHF-tau in AD brains (Wolozin et al., 1986; Papasozomenos, 1989; Lee et al., 1991; Watanabe et al., 1992), the appearance of Alz50-positive neurons (Uchihara et al., 1995) and of tau2-positive microglia (Uchihara et al., 2000) around the ischemic area even in the absence of phosphorylated tau indicates that the conformational changes in tau induced by ischemia mimic PHF-tau at the tau2 epitope but are not extended to other epitopes. Because tau2 was initially raised against bovine tau, it is reasonable that this antibody exhibits higher affinity for bovine tau than for human tau (Fig. 6) (Papasozomenos and Binder, 1987). Ser101 of bovine tau, at the center of this synthetic peptide (AGIGDTS*NLEDQAA) as indicated by the asterisk, was reported to be crucial for its affinity for tau2, and this Ser-like conformation, mimicked by its human counterpart Pro, represents pathological conformation of the tau2 epitope integrated in NFTs (Watanabe et al., 1992). Replacement

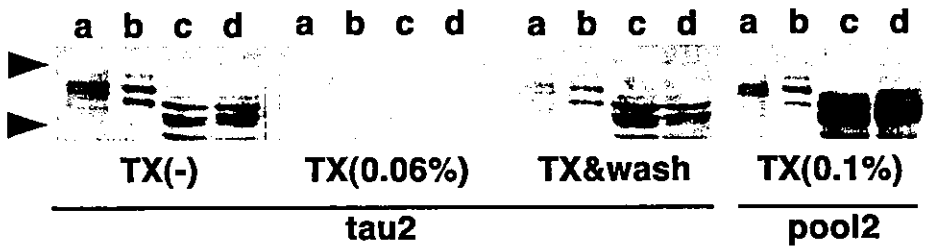

Fig. 7. Fractions containing tau-immunoreactive bands (a, SDS-soluble fraction from AD; b, PHF fraction from AD; c, Tris-soluble fraction from infarction; d, Tris-soluble fraction from normal control) were subjected to 10% SDS-PAGE and probed with tau2 or pool2. Tau2-immunoreactive bands, detectable when incubated with tau2 in the absence of TX [TX(−)], disappeared when incubated with tau2 in the presence of 0.06% TX [TX(0.06%)]. Suppressed tau2-immunoreactive bands were restored after washing (TX&wash) and were visualized with pool2 even in the presence of TX at a higher concentration [TX(0.1%)]. Upper arrowhead, 68 kDa; lower arrowhead, 50 kDa.

of this Ser with Pro, as seen in the corresponding sequence of human tau, is associated with a change in the conformation of this fragment detectable on CD spectra (Lang and Otvos, 1992) and in its reduced affinity for tau2 (Watanabe et al., 1992). Higher affinity of PHF-tau for tau2 is explained if human tau protein undergoes conformational change centered at this Pro to mimic Ser-like conformation (Watanabe et al., 1992; Carmel et al., 1996). Because the antigen peptide mimicking this Ser-like conformation reduced the tau2 IR not only in NFTs but also in microglial cells around ischemic foci, tau proteins in these pathological structures share this conformational change. This indicates again that this conformational change in the tau2 epitope, seen in microglial cells around ischemic foci and in GCIs (Shibuya et al., 2003), is not necessarily linked to phosphorylation of tau or PHF formation.

The copresence of TX with tau2 abolished these tau2-immunoreactive bands in a reversible fashion on brain homogenates from human brains regardless of the diagnoses, whereas affinity of tau2 for bovine tau was less affected, probably because its original Ser101 conformation is retained. This relative resistance to TX was shared with NFTs only when observed on fixed histological sections, suggesting that the organization of tau into PHF confers some stability on this tau2 epitope. Because this relative resistance to TX was observed neither on solubilized PHF-tau subjected to SDS-PAGE nor on tau from ischemic foci devoid of a fibrillary structure, it is probably related to the fibrillary structure remaining as NFTs on fixed sections, which, however, should have been destroyed during solubilization for SDS-PAGE.

Although this modification of tau2 epitope is shared by GCIs (Shibuya et al., 2003), NFTs of AD, and microglial cells around ischemic foci, immunohistochemical visualization with other antitau antibodies, which immunolabel NFTs without exception, was unsuccessful on these microglial cells and GCIs (Shibuya et al., 2003). This suggests that the modified portion of tau after ischemic insults is not sufficiently extended to involve other tau epitopes, as was seen on GCIs (Shibuya et al., 2003). It is therefore interesting if this modification of tau2 epitope seen in microglia is similar to early stage of NFT formation not associated with fibril formation or with immunohistochemical visualization of other tau epitopes (Benzing and Mufson, 1995). Moreover, exclusive visualization of tau2, but not other tau epitopes, on histological sections has been described in some cases with a degenerative process characterized by ubiquitin-positive neuronal inclusions (Kertesz et al., 2000; Forno et al., 2002). It remains to be proved, however, whether selective immunohistochemical visualization of tau2 epitope reported in these degenerative processes (Kertesz et al., 2000; Forno et al., 2002) is just a nonspecific reaction of tau2 or represents a specific IR as we confirmed on microglial cells around ischemic foci and on GCIs (Shibuya et al., 2003). Nevertheless, we are reluctant to apply the term "tauopathy" to describe tau deposition seen in ischemic foci, even though tau deposition is extensive, because immunohistochemical visualization of tau2 epitope is apparently secondary to ischemic insult and because tau deposits are not organized into fibrils or more solid inclusions. It is therefore supposed that further steps or distinct cascades of tau modification will be necessary to generate fibrillary structures like NFTs.

Although simple immunohistochemical visualization of tau is not enough to distinguish different types of tau deposits, selective modification of tau2 epitope and the susceptibility of tau2 epitope to TX, as we demonstrated in this study, will provide an additional feature in characterizing tau deposition in glial cells, which is common to microglia in ischemia and GCIs in oligodendroglia. Further studies to clarify the molecular basis to explain possible conformational changes in the tau2 epitope induced by ischemia and its characteristic features distinct from other degenerative tauopathies will be necessary to disclose modifications of tau protein specific for each pathological process.

ACKNOWLEDGMENTS

The authors thank Professors Y. Ihara (University of Tokyo) and P. Davies (Albert Einstein University) for kindly supplying antihuman tau (pool2) antibody and Alz-50, respectively. They are grateful to Dr. Ray Cowan for reading the article. Supported in part by the Ministry of Health and Welfare (Longevity Science

H-14-005) and the Ministry of Education, Culture, Sports, Science and Technology (grant in aid for scientific research B15300118) to T.U.

REFERENCES

Arai T, Ikeda K, Akiyama H, Tsuchiya K, Yagishita S, Takamatsu J. 2001. Intracellular processing of aggregated tau differs between corticobasal degeneration and progressive supranuclear palsy. Neuroreport 12:935–938.

Benzing WC, Mufson EJ. 1995. Apolipoprotein E immunoreactivity within neurofibrillary tangles: relationship to tau and PHF in Alzheimer's disease. Exp Neurol 132:162–171.

Burkhart KK, Beard DC, Lehman RAW, Billingsley ML. 1998. Alteration in tau phosphorylation in rat and human neocortical brain slices following hypoxia and glucose deprivation. Exp Neurol 154: 464–472.

Carmel G, Mager EM, Binder LI, Kuret J. 1996. The structural basis of monoclonal antibody Alz50's selectivity for Alzheimer's disease pathology. J Biol Chem 51:32789–32795.

Dewar D, Graham DI, Teasdale GM, McCulloch J. 1993. Alz-50 and ubiquitin immunoreactivity is induced by permanent focal cerebral ischemia in the cat. Acta Neuropathol 86:623–629.

Dewar D, Dawson D. 1995. Tau protein is altered by focal cerebral ischaemia in the rat: an immunohistochemical and immunoblotting study. Brain Res 684:70–78.

Endoh R, Ogawara M, Iwatsubo T, Nakano I, Mori H. 1993. Lack of carboxy terminal sequence of tau in ghost tangles of Alzheimer's disease. Brain Res 601:164–172.

Forno LS, Langston JW, Herrick MK, Wilson JD, Murayama S. 2002. Ubiquitin-positive neuronal and tau 2-positive glial inclusions in frontotemporal dementia of motor neuron type. Acta Neuropathol 130:599–606.

Geddes JW, Schwab C, Craddock S, Wilson JL, Pettigrew LC. 1994. Alterations in tau immunostaining in the rat hippocampus following transient cerebral ischemia. J Cereb Blood Flow Metab 14:554–564.

Goedert M, Spillantine MG, Cairns NJ, Crowther RA. 1992. Tau proteins of Alzheimer paired helical filaments: abnormal phosphorylation of all six brain isoforms. Neuron 8:159–168.

Greenberg S, Davies P. 1990. A preparation of Alzheimer paired helical filaments that displays distinct tau proteins by polyacrylamide gel electrophoresis. Proc Natl Acad Sci USA 87:5827–5831.

Irving EA, Nicoll J, Graham DI, Dewar D. 1996. Increased tau immunoreactivity in oligodendrocytes following human stroke and head injury. Neurosci Lett 213:189–192.

Irving EA, Yatsushiro K, McCulloch J, Dewar D. 1997. Rapid alteration of tau in oligodendrocytes after focal ischemic injury in the rat: involvement of free radicals. J Cereb Blood Flow Metab 17:612–622.

Kertesz A, Kawarai T, Rogaeva E, St. George-Hyslop P, Poorkaj P, Bird TD, et al. 2000. Familial frontotemporal dementia with ubiquitin-positive, tau-negative inclusions. Neurology 54:818–827.

Lang E, Otvos L. 1992. A serine→proline change in the Alzheimer's disease-associated epitope tau2 results in altered secondary structure, but phosphorylation overcomes the conformational gap. Biochem Biophys Res Com 188:162–169.

Lee VM-Y, Balin BJ, Otvos L, Trojanowski JQ. 1991. A68: a major subunit of paired helical filaments and derivatized forms of normal tau. Science 251:675–678.

Lee VM, Goedert M, Trojanowski JQ. 2001. Neurodegenerative tauopathies. Ann Rev Neurosci 24:1121–1159.

Matsuo ES, Shin R-W, Billingsley ML, Van deVoorde A, O'Connor M, Trojanowski JQ, et al. 1994. Biopsy-derived adult human brain tau is phosphorylated at many of the same sites as Alzheimer's disease paired helical filament tau. Neuron 13:989–1002.

Mercken M, Vandermeeren M, Lübke U, Six J, Boons J, Van de Voorde A, et al. 1992. Monoclonal antibodies with selective specificity for Alzheimer tau are directed against phophatase-sensitive epitopes. Acta Neuropathol 84:265–272.

Odawara T, Iseki E, Kosaka K, Akiyama H, Ikeda K, Yamamoto T. 1995. Investigation of tau-2 positive microglia-like cells in the subcortical nuclei of human neurodegenerative disorders. Neurosci Lett 192:145–148.

Papasozomenos SC, Binder LI. 1987. Phosphorylation determines two distinct species of tau in the central nervous system. Cell Motil Cytoskel 8:210–226.

Papasozomenos SC. 1989. Tau protein immunoreactivity in dementia of the Alzheimer type: I, morphology, evolution, distribution, and pathogenetic implications. Lab Invest 60:123–137.

Papasozomenos SC, Su Y. 1991. Altered phosphorylation of tau protein in heat-shocked rats and patients with Alzheimer disease. Proc Natl Acad Sci USA 88:4543–4547.

Pollock NJ, Wood JG. 1988. Differential sensitivity of the microtubule associated protein, tau, in Alzheimer's disease tissue to formalin fixation. J Histochem Cytochem 36:1117–1121.

Shackelford DA, Nelson KE. 1996. Changes in phosphorylation of tau during ischemia and reperfusion in the rabbit spinal cord. J Neurochem 66:286–295.

Shackelford DA, Yeh RY. 1998. Dephosphorylation of tau during transient forebrain ischemia in the rat. Mol Chem Neuropathol 34:103–120.

Shibuya K, Uchihara T, Nakamura A, Ishiyama M, Yamaoka K, Yagishita S, et al. 2003. Reversible conformational change of tau-2 epitope exposed to detergent in glial cytoplasmic inclusions in multiple system atrophy. Acta Neuropathol 105:508–514.

Uchihara T, Tsuchiya K, Kondo H, Hayama T, Ikeda K. 1995. Widespread appearance of Alz-50 immunoreactive neurons in the human brain with cerebral infarction. Stroke 26:2145–2148.

Uchihara T, Tsuchiya K, Nakamura A, Ikeda K. 2000. Appearance of tau-2 immunoreactivity in glial cells in human brain with cerebral infarction. Neurosci Lett 286:99–102.

Watanabe N, Takio K, Hasegawa M, Arai T, Titani K, Ihara Y. 1992. Tau 2: a probe for a Ser conformation in the amino terminus of tau. J Neurochem 58:960–966.

Wolozin BL, Pruchnicki A, Dickson DW, Davies P. 1986. A neuronal antigen in the brains of Alzheimer's patients. Science 232:648–650.

Volume 51(9): 1201–1206, 2003
The Journal of Histochemistry & Cytochemistry
http://www.jhc.org

ARTICLE

Triple Immunofluorolabeling with Two Rabbit Polyclonal Antibodies and a Mouse Monoclonal Antibody Allowing Three-dimensional Analysis of Cotton Wool Plaques in Alzheimer Disease

Toshiki Uchihara, Ayako Nakamura, Hiroshi Nakayama, Kunimasa Arima, Norio Ishizuka, Hiroshi Mori, and Setsuo Mizushima

Departments of Neuropathology (TU,AN) and Brain Structure (NI), Tokyo Metropolitan Institute for Neuroscience, Tokyo, Japan; Department of Psychiatry, Tokyo Metropolitan Neurological Hospital, Tokyo, Japan (HN); Department of Laboratory Medicine, National Center Hospital for Mental, Nervous, and Muscular Disorders, National Center for Neurology and Psychiatry, Tokyo, Japan (KA); Department of Neuroscience, Osaka City University School of Medicine, Osaka, Japan (HM); and Mizushima Clinic, Tokyo, Japan (SM)

SUMMARY We established a triple-labeling method with two rabbit polyclonal antibodies and a mouse monoclonal antibody and examined autopsied brain tissue with cotton wool plaques (CWPs). One of the polyclonal antibodies was so diluted (anti-Aβ42 or anti-Aβ40/1:30,000 or anti-von Willebrand factor/1:1000) that its visualization was possible only after amplification with the catalyzed reporter deposition (CARD) method. The other polyclonal antibody (anti-Aβ40 or anti-Aβ42/1:1000) was visualized with a fluorochrome conjugated to an anti-rabbit antibody that specifically visualized the latter polyclonal antibody because of its lower sensitivity. A monoclonal antibody, AT8, was superimposed to yield triple immunofluorolabeling. Serial optical sections with an interval of 0.3 μm were reconstructed to allow three-dimensional (3D) observation of these three epitopes. Aβ40 was localized to core-like structures, mainly in layers I–III, and was sometimes in contact with the vascular wall, both without neuritic reactions. CWPs, present in layers I–VI, were labeled with anti-Aβ42 and were accompanied by neuritic reactions. These differences suggest that mechanisms of Aβ deposition and its relation to neuritic reactions or to blood vessels differ according to the lesion, even in the same microscopic field.

(J Histochem Cytochem 51:1201–1206, 2003)

KEY WORDS
triple immunofluorescence
three dimensions
reconstruction
laser confocal microscopy
amyloid
Aβ42
cotton wool plaques

THE COTTON WOOL PLAQUE (CWP) is a peculiar type of senile plaque seen in brains of some patients with familial Alzheimer disease (AD) and in those of sporadic AD. CWPs are characterized by robust deposition of amyloid β protein (Aβ), Aβ42 (Crook et al. 1998; Le et al. 2001; Steiner et al. 2001; Verkkoniemi et al. 2001; Tabira et al. 2002), a longer molecular species of Aβ, possibly involved in early phase of Aβ deposition (Iwatsubo et al. 1994). Although its shorter counterpart Aβ40 is also another major constituent of senile plaques, the spatial relationship between these Aβ species and other components is of particular interest because deposition of each Aβ species is considered to occur at different stages of senile plaque formation (Iwatsubo et al. 1994). By immunizing rabbits, one of the authors (HM) has generated anti-Aβ antibodies, each of which specifically reacts with either Aβ42 or Aβ40 (Akiyama et al. 1997). We wanted to examine the spatial relationship between these two epitopes specifically detectable with these antibodies by using multi-labeling immunohistochemistry (Van der Loos et al. 1989; Uchihara et al. 1995,2000).

One of the obstacles was that the antibodies to be applied on the same sections were from the same spe-

Correspondence to: Toshiki Uchihara, Dept. of Neuropathology, Tokyo Metropolitan Institute for Neuroscience, 2-6 Musashidai, Fuchu, Tokyo 183-8526, Japan. E-mail: uchihara@tmin.ac.jp
Received for publication November 5, 2002; accepted April 2, 2003 (2A5958).

0022-1554/03/$3.30

cies, which usually hampers multilabeling. Several procedures have been proposed to circumvent this difficulty, with some success. For example, conjugation of enzyme, biotin, or fluorochrome to one of the primary antibodies allows separate detection of the two antibodies, but it requires a relatively large amount of the antibody and the conjugation procedure can be cumbersome (Van der Loos et al. 1989; Uchihara et al. 1995). Another approach is to wash out the bound antibodies with glycine buffer at very low pH after the first cycle of immunodetection (Nakane 1968). Treatment in a microwave oven after the color development of the first primary antibody has been reported to be effective in avoiding crossreaction (Lan et al. 1995). Although these sequential procedures are generally successful in detecting non-co-localizing epitopes, they are not applicable for multiple immunofluorescence labeling.

A previous study demonstrated that double immunofluorolabeling with two antibodies from the same species was possible with extensive blockade with $F(ab')_2$ fragment (Lewis–Carl et al. 1993) between the two primary antibodies. However, double labeling with this method was associated with a significant decrease in the sensitivity of one of the primary antibodies applied after this extensive blocking. This trade-off of double labeling with decreased sensitivity was circumvented when one of the antibodies was amplified (Hunyady et al. 1996) with the catalyzed reporter amplification method (CARD). CARD amplification is mediated by the horseradish peroxidase (HRP) on the secondary antibody that catalyzes the activation of tyrosine bound to biotin (Bobrow et al. 1989). The activated tyrosine becomes attached to proteins in the tissue section at the site of the antigen–antibody reaction. Biotin bound to tyrosine can then be visualized (Adams 1992). With this method, discrimination of the two epitopes is possible based on the different sensitivity of the immunodetection systems either with or without the amplification. The first antibody to be used must be diluted below the level detectable with standard secondary antibody labeled with fluorochrome, but above the level detectable with CARD amplification (Hunyady et al. 1996). In the present study we used two different polyclonal antibodies produced in rabbits to visualize two different epitopes possibly co-localizing with each other on the same structure, Aβ40/Aβ42, and Aβ40/von Willebrand factor (a specific marker for vascular endothelial cells). The third antibody, AT8, a mouse monoclonal antibody (MAb) against paired helical filaments (PHFs), major components of neurofibrillary tangles and neurites (Mercken et al. 1992), can be combined by using a differently labeled secondary antibody specific for mouse IgG without danger of crossreaction with these polyclonal antibodies.

In observing structures, such as senile plaques, that exceed the thickness (5–10 μm) of routine histological sections, we are not sure whether or not portions included in the section under observation represent the entire structure. We therefore obtained serial optical sections under a laser scanning confocal microscope to be reconstructed for 3D observation. Three-dimensional reconstruction of triple-labeled sections, as we established in this study, can provide an opportunity to observe the entire structure of CWPs and the spatial relationship between the relevant structures.

Materials and Methods

A dementia patient with a familial background of Alzheimer disease was diagnosed with AD based on the presence of many senile plaques and neurofibrillary tangles. Senile plaques in this case were not clearly detectable with the Bodian method, but hematoxylin and eosin staining visualized the cotton wool feature of the plaques without a core. In addition, a core-like structure and perivascular deposits of Aβ were observed (Nakayama et al. 2001; Tabira et al. 2002). The genetic abnormality associated with this phenotype remains to be clarified.

We first undertook experiments to establish the optimal concentrations of the antibodies for the methods used, especially the dilution of the primary antibodies visualized with the CARD method but undetectable by the standard method without CARD amplification. The list of primary antibodies is provided in Table 1. Three-μm-thick mirror sections were obtained from formalin-fixed, paraffin-embedded blocks from the occipital lobe of this patient. Deparaffinized sections were treated with formic acid (>99%) for 5 min to enhance Aβ-like immunoreactivity (Kitamoto et al. 1987). After being treated with 2% H_2O_2 and incubation with 5% bovine serum albumin in PBS, sections were incubated at 4C for 2 days with different concentrations (1:1000–1:100,000) of anti-Aβ40 or anti-Aβ42 antibody (Akiyama et al. 1997). One of the mirror sections was visualized after amplification with CARD as previously described (Bobrow et al. 1989; Adams 1992; Uchihara et al. 2000). Briefly, after application of an anti-rabbit IgG made in goat conjugated to horseradish peroxidase (HRP, 1:500; Pierce, Rockford, IL), the HRP signal was amplified with biotinylated tyramide (1:1000; Perkin–Elmer, Boston, MA) and was finally visualized with FITC conjugated to streptavidin (1:200; Vector, Burlingame, CA; Uchihara et al. 2000). The counterpart of the mirror section was visualized with anti-rabbit IgG made in goat conjugated with FITC (1:200; Vector).

For triple immunofluorolabeling, deparaffinized sections were similarly subjected to immunolabeling with CARD amplification with one of the polyclonal antibodies made in rabbits (anti-Aβ42 1:30,000; anti-Aβ40 1:30,000; or anti-von Willebrand factor 1:1000; DAKO, Glostrup, Denmark) as described above and finally visualized to Cy5 conjugated to streptavidin (1:200; Kirkegaard & Perry, Gaithersburg, MD). von Willebrand factor is a marker for vascular endothelial cells and the anti-von Willebrand factor antibody im-

Table 1 Antibodies and optimal dilutions used in this study

Epitope	Designation or clone	Dilution (CARD+/−)[a]	Species (class)	Source
Aβ40	Aβ40[b]	30,000/1000	Rabbit (IgG)	H. Mori
Aβ42	Aβ42[b]	30,000/1000	Rabbit (IgG)	H. Mori
PHF-tau	AT8[c]	−/1000	Mouse (IgG)	Innogenetics
von Willebrand factor	A082	1000/−	Rabbit (IgG)	DAKO

[a]CARD+/−, optimal dilution of the antibody with/without CARD amplification.
[b]Akiyama et al. 1997.
[c]Mercken et al. 1992.

munolabels blood vessels (Uchihara et al. 1995). The sections were then incubated with a mixture of AT8 (1:1000; mouse monoclonal antibody against PHFs; Innogenetics, Zwijndrecht, Belgium) and another polyclonal antibody (anti-Aβ40 or anti-Aβ42 1:1000) at 4C for another 2 days in the dark. These two antibodies were visualized with a mixture of anti-mouse IgG made in sheep conjugated with rhodamine (1:200; Jackson ImmunoResearch, West Grove, PA) and anti-rabbit IgG made in goat conjugated with FITC (1:200; Vector), respectively.

For 3D observation, formalin-fixed blocks were washed in PBS and cryoprotected by being soaked in 20% sucrose buffered with 0.1 M phosphate. Thick floating sections (50–100-μm in thickness) were obtained on a freezing microtome. They were subjected to the triple-immunolabeling method as above with prolonged incubation (up to 7 days) with the primary antibody. Sections were mounted with 90% glycerol in 0.1 M phosphate buffer containing 0.1% of *p*-phenylenediamine and were observed under a confocal laser scanning microscope (Leica TCS/SP; Heidelberg, Germany). Excitation of the fluorochromes and their maximal detection wavelength are summarized in Table 2. Serial optical sections were obtained and reconstructed for 3D analysis on software (TRI/3D; Ratoc System, Tokyo, Japan).

Results

Serial dilution of one of the polyclonal antibodies (anti-Aβ40) demonstrated that the usual immunofluorescence method without CARD amplification (Figures 1A, 1C, 1E, and 1G) requires a high concentration of the antibody (1:1000) to obtain maximal labeling (Figure 1C). However, CARD amplification (Figures 1B, 1D, 1F, and 1H) enabled us to use the antibody at lower concentrations (up to 1:30,000) to obtain a clear fluorescent signal of an equivalent intensity with little background staining (Figure 1F).

Table 2 Fluorescent dyes and their link to epitopes

Dye	Excited at (nm)	Detected between (nm)	Conjugated molecule	Target epitope	Displayed as
FITC	488	500–530	Anti-rabbit IgG	Aβ40(Aβ42)	Green
Rhodamine	568	590–630	Anti-mouse IgG	AT8	Red
Cy5	648	700–750	Streptavidin	Aβ42(Aβ40)	Blue

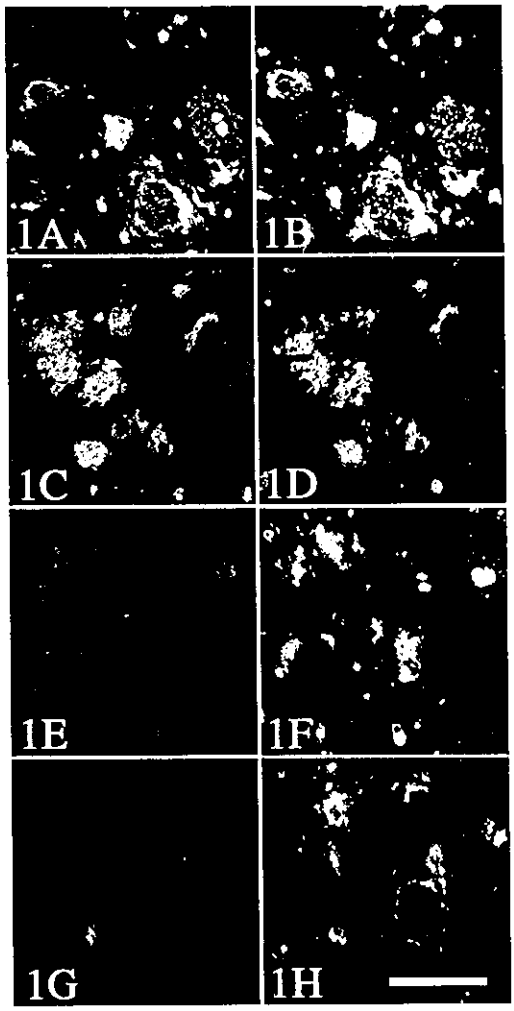

Figure 1 Immunolabeling of mirror-section pairs from cerebral cortex with anti-Aβ40 at dilution 1:1000 (**A,B**), 1:10,000 (**C,D**), 1:30,000 (**E,F**), and 1:100,000 (**G,H**) visualized without (**A,C,E,G**) and with (**B,D,F,H**) CARD amplification. At dilution 1:30,000, labeling after CARD amplification visualized Aβ40 deposits (**F**), but that without the amplification failed to exhibit labeling (**E**). Bar = 100 μm.

Omission of either primary antibody, secondary antibody, or biotinylated tyramide completely eliminated the immunofluorescent signal. Similar results were obtained with the anti-Aβ42 antibody (data not shown).

Therefore, we first performed CARD-amplified immunofluorolabeling with anti-Aβ40 (Figures 2A–2C), which was visualized with Cy5, shown as blue. Subsequent double labeling with AT8 (1:1000; Figures 2A–2C, red) and with anti-Aβ42 (1:1000; Figures 2A and 2C, green) antibody was visualized with the mixture of anti-mouse IgG conjugated with rhodamine and anti-rabbit IgG conjugated with FITC. As shown in Figure 2, no crossreaction between the two rabbit polyclonal antibodies (anti-Aβ40 and anti-Aβ42) was detectable. Moreover, it is noteworthy that reverse ex-

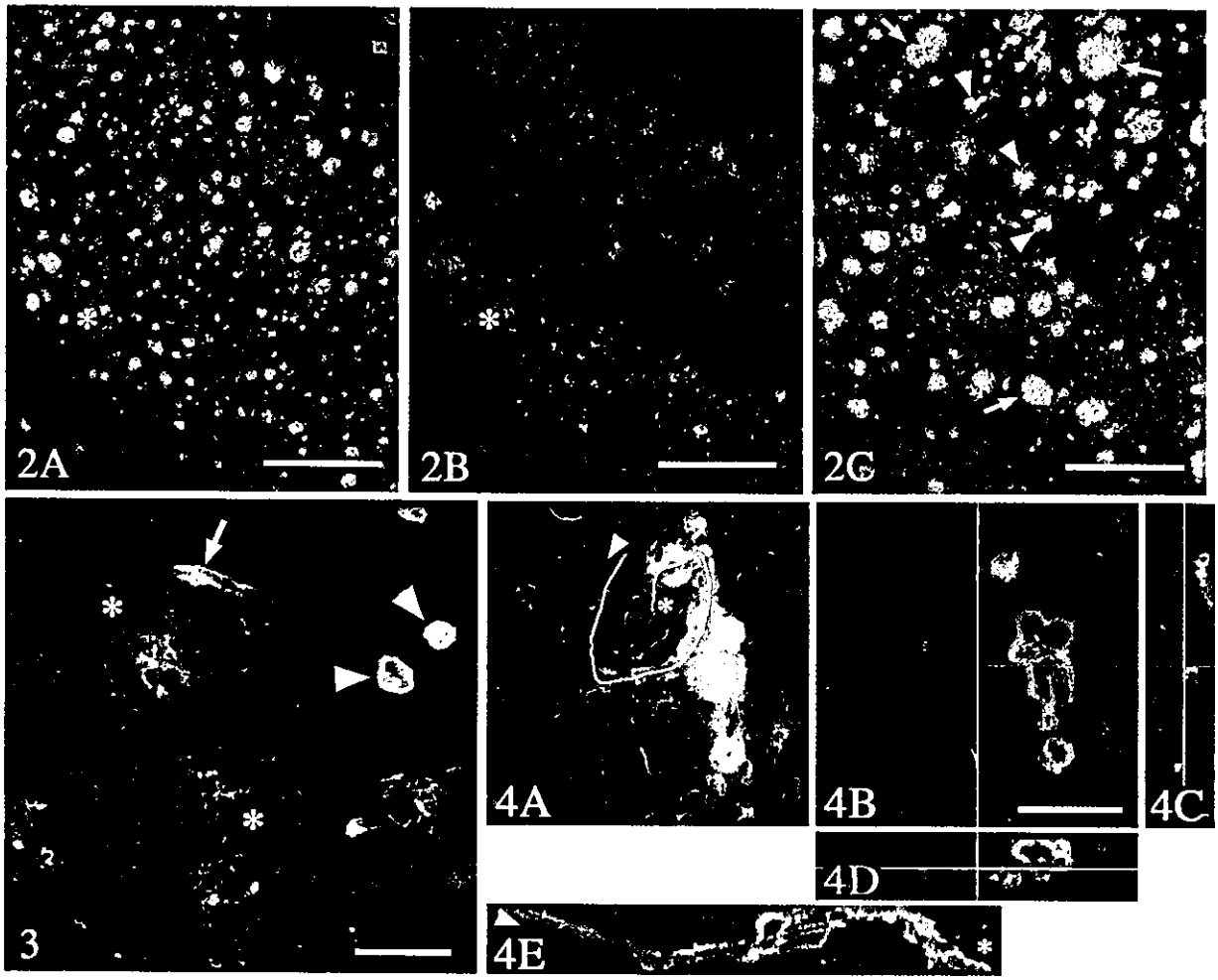

Figure 2 (A) Cerebral cortex (pial surface, right upper corner; white matter, left lower corner) immunofluorolabeled with anti-Aβ42 (green), anti-Aβ40 (blue), and anti-PHF (red). Large deposits of Aβ42 are scattered without specific laminar distribution. (B) The same field as A. Immunolabeling with anti-Aβ42 is deleted from A. Laminar distribution of neurofibrillary tangles is evident. Deposits of Aβ40 are rare in the deep layers (asterisk), where deposits of Aβ42 are numerous (A). Bars = 500 μm. (C) Higher magnification of A. Core-like structures (arfowheads) are positive for both Aβ40 and Aβ42, whereas large cotton wool plaques are mainly positive for Aβ42 (arrows). Bar = 250 μm.

Figure 3 Triple immunofluorolabeling of the cerebral cortex with anti-Aβ42 (blue), anti-Aβ40 (green), and anti-PHF tau (red). Cotton wool plaques (asterisks) are positive mainly for Aβ42, and participation of Aβ40 is not detectable. Core-like structures (arrowheads) and blood vessel (arrow) are positive for Aβ40 and for Aβ42 to a lesser extent. Reactive neurites are slender and are clustered around CWPs but are not detectable around Aβ40-positive structures. Bar = 100 μm.

Figure 4 A total of 114 optical sections (X–Y with the interval of 0.3 μm along Z-axis) were obtained from a triple-labeled thick floating section (green, Aβ40; red, PHF-tau; blue, von Willebrand factor for blood vessels) from the cerebral cortex. Three-dimensional reconstruction was performed on the software. (A) Stacked image of the 114 optical sections (X–Y). Core-like structures (Aβ40) were clustered along the blood vessel. (B) One of the optical sections (X–Y) at the depth indicated with white lines in C and D. (C) Cross-sectional Y–Z image along the yellow lines indicated in B and D. (D) Cross-sectional X–Z image along the red line indicated in B and C. (E) Cross-sectional image along the blood vessel indicated with a white arbitrary line in A with two extremities marked as arrowhead and asterisk. Focal deposition of Aβ40 in the vessel wall was occasionally in continuity with core-like structures around the vessel wall. Bar = 50 μm.

periments, anti-Aβ42 with amplification followed by anti-Aβ40, gave essentially the same results (Figure 3).

Most of the CWPs were homogeneously labeled with the anti-Aβ42 antibody [green in Figure 2 (arrows) and blue in Figure 3], and participation of Aβ40 was partial on these CWPs (blue in Figure 2 and green in Figure 3). In contrast, Aβ40 was deposited as core-like structures (arrowheads in Figures 2C and 3), which were rare in deeper layers of the cerebral cortices (asterisk in Figure 2B, blue) and contained also Aβ42 (arrowheads in Figure 2C). Three-dimensional analysis demonstrated that these core-like structures positive for Aβ40 (Figure 4, green) were sometimes clustered along the blood vessel (arrowhead in Figure

4A). The Aβ40 epitope was sometimes co-localized to the vessel wall, with an occasional continuity to these core-like structures. Neuritic reactions, detected with AT8/rhodamine, were present around CWPs (asterisks in Figure 3, red), but they were rarely observed around the core-like structures (arrowheads in Figure 3) or the vessel wall (arrow in Figure 3).

As suggested by the stacked view of the 114 optical sections (Figure 4A), some of the core-like structures were occasionally clustered around blood vessels. Three-dimensional observation with the software enabled us to examine a simultaneous stereoscopic view of these three epitopes (Aβ40, PHF-tau, and blood vessel). Finally, a cross-sectional view along an arbitrary cutting line on the blood vessel (from arrowhead to asterisk in Figure 4) showed that Aβ40 accumulated around the blood vessel either in a linear or a spherical fashion (Figure 4E).

Discussion

We successfully performed triple immunofluorolabeling with two antibodies raised in rabbits and another mouse MAb. Single immunofluorolabeling with different concentrations of the anti-Aβ40 antibody clarified that the optimal dilution of the anti-Aβ antibodies without CARD amplification was 1:1000, whereas equivalent labeling was obtained at a dilution of 1:30,000 after amplification with CARD. One of the theoretical bases for discriminating two distinct epitopes with antibodies raised in the same species depends on this difference in the optimal concentration of the antibody for immunofluorescence study (Hunyady et al. 1996). The anti-Aβ40 antibody in the first cycle was so diluted (1:30,000) that the corresponding epitope could be visualized only after the amplification, but visualization without amplification, as used in the second cycle, was not sensitive enough to detect this anti-Aβ40 antibody diluted further to another 30-fold below the detection threshold. It is possible that the anti-rabbit antibody used in the first cycle before CARD amplification could be a source of crossreaction because it has an affinity for the other polyclonal antibody produced also in rabbit used in the second cycle. Practically, this reaction was found to be less than the detection threshold, as demonstrated in Figure 2, which showed definite separation of the signals from Aβ40 and Aβ42 epitopes. Specific labelings were perfectly interchangeable when the two antibodies, anti-Aβ40 and anti-Aβ42, were replaced with each other (Figure 3), which provided additional evidence that crossreaction between the two epitopes was negligible. The absence of crossreaction may be explained by the low concentration of the first primary antibody, which attracts, if any, a very tiny amount of the anti-rabbit antibody. This amount of the anti-rabbit antibody should be far below the detection threshold even if the second polyclonal antibody is attached to it. Wide separation of the emission signals from FITC and from Cy5 made it possible to insert another emission signal from rhodamine without crosstalk between them (Table 2), because rhodamine was designed to label another monoclonal antibody, AT8, through anti-mouse IgG, which never crossreacts with the other two polyclonal antibodies produced in rabbits.

These triple-labeled sections demonstrated that most of the CWPs were homogeneously stained with the anti-Aβ42 antibody (Crook et al. 1998; Le et al. 2001; Steiner et al. 2001; Verkkoniemi et al. 2001; Tabira et al. 2002). One of the intriguing findings was that core-like structures were intensely labeled with the anti-Aβ40 antibody. These core-like structures were rare in deeper cortical layers of the cerebral cortex (Figure 2B) and were not necessarily associated with deposits of Aβ42. Although a possible spatial relationship of these core-like structures to blood vessels was suspected even with two-dimensional observation (Figure 3), 3D reconstruction confirmed that they were sometimes in continuity with blood vessels similarly labeled with the anti-Aβ40 antibody (Figure 4). Furthermore, this reconstruction enabled us to observe cross-sectional images not only along the X, Y, or Z axis but also along an arbitrary line tracing the target structure, e.g., blood vessels as shown in Figure 4E. No similar relationship to blood vessels was evident with Aβ42-positive CWPs. Simultaneous labeling with AT8/rhodamine demonstrated that AT8-positive neurites were slender, without focal swelling, and were abundant around CWPs but rarely associated with the core-like structures. Furthermore, AT8-positive structures were uniformly scattered throughout the entire thickness of the sections, providing proof that this triple immunofluorolabeling reliably and homogeneously detected the structures in question under the present experimental conditions applied to the thick sections. Morphology, immunohistochemical features, and association of tau-positive neurites were found to be different in Aβ42-positive CWPs from those in Aβ40-positive core-like structures and blood vessels. These differences suggest that mechanisms involved in Aβ deposition may be different in these structures found in the same microscopic field.

In summary, we established a triple-immunofluorolabeling method with two rabbit polyclonal antibodies and a mouse monoclonal antibody, which simultaneously visualized Aβ40, Aβ42, or von Willebrand factor and PHF-tau epitopes. Application of this triple immunofluorolabeling enabled thick sections to be analyzed on a 3D basis. Immunohistochemical features and distribution were found to be different between Aβ42-positive deposits and their Aβ40-positive counterparts. This suggests that the mechanism of Aβ

deposition for CWPs is different from that of other Aβ deposits, such as core-like structures. This triple-labeling method will expand the applicability and precision of multiple immunoflurolabeling, which is advantageous in a wide range of research and diagnosis.

Acknowledgments

Supported in part by a grant (TU) from the Ministry of Culture, Sports, Science and Technology, Japan.

We are grateful to Mr Ray Cowan for reading the manuscript.

Literature Cited

Adams JC (1992) Biotin amplification of biotin and horseradish peroxidase signals in histochemical stains. J Histochem Cytochem 40:1457–1463

Akiyama H, Mori H, Sahara N, Kondo H, Ikeda K, Nishimura T, Oda T, et al. (1997) Variable deposition of amyloid β-protein (Aβ) with the carboxy-terminus that ends at residue valine 40 (Aβ40) in the cerebral cortex of patients with Alzheimer's disease: a double-labeling immunohistochemical study with antibodies specific for Aβ40 and the Aβ that ends at residues alanine 42/threonine43 (Aβ42). Neurochem Res 22:1499–1506

Bobrow MN, Harris TD, Shaughnessy KJ, Litt GJ (1989) Catalyzed reporter deposition, a novel method of signal amplification. Application to immunoassays. J Immunol Methods 125:279–285

Crook R, Verkkoniemi A, Perez-Tur J, Mehta N, Baker M, Houlden H, Farrer M, et al. (1998) A variant of Alzheimer's disease with spastic paraparesis and unusual plaques due to deletion of exon 9 of presenilin 1. Nature Med 4:452–455

Hunyady B, Krempels K, Harta G, Mezey E (1996) Immunohistochemical signal amplification by catalyzed reporter deposition and its amplification in double immunostaining. J Histochem Cytochem 44:1353–1362

Iwatsubo T, Odaka A, Suzuki N, Mizusawa H, Nukina N, Ihara Y (1994) Visualization of A beta 42(43) and A beta 40 in senile plaques with end-specific A beta monoclonals: evidence that an initially deposited species is A beta 42(43). Neuron 13:45–53

Kitamoto T, Ogomori K, Tateishi J, Prusiner SB (1987) Formic acid pretreatment enhances immunostaining of cerebral and systemic amyloids. Lab Invest 57:230–236

Lan HY, David WM, Nikolic-Paterson DJ, Atkins RC (1995) A novel, simple, reliable, and sensitive method for multiple immunoenzyme staining: use of microwave oven heating to block antibody crossreactivity and retrieve antigens. J Histochem Cytochem 43:97–102

Le TV, Crook R, Hardy J, Dickson DW (2001) Cotton wool plaques in non-familial late-onset Alzheimer disease. J Neuropathol Exp Neurol 60:1051–1061

Lewis-Carl SAL, Gillete-Ferguson I, Ferguson DG (1993) An indirect immunofluorescence procedure for staining the same cryosection with two mouse monoclonal primary antibodies. J Histochem Cytochem 41:1273–1278

Mercken M, Vandermeern M, Lübke U, Six J, Boons J, Van de Voorde A, Martin J-J, et al. (1992) Monoclonal antibodies with selective specificity for Alzheimer tau are directed against phosphatase-sensitive epitopes. Acta Neuropathol (Berl) 84:265–272

Nakane PK (1968) Simultaneous localization of multiple tissue antigens using the peroxidase labeled antibody method. A study on pituitary gland of the rat. J Histochem Cytochem 16:557–560

Nakayama H, Arima K, Mizushima S, Chui DH, Tabira T (2001) An autopsy case of juvenile Alzheimer's disease with cotton wool plaques. Neuropathology 21(suppl):A32

Steiner H, Revesz T, Neumann M, Romig H, Grim MG, Pesold B, Kretzschmar HA, et al. (2001) A pathogenic presenilin-1 deletion causes aberrant Aβ42 production in the absence of congophilic amyloid plaques. J Biol Chem 276:7233–7239

Tabira T, Chui DH, Nakayama H, Kuroda S, Shibuya M (2002) Alzheimer's disease with spastic paraparesis and cotton wool type plaques. J Neurosci Res 70:367–372

Uchihara T, Kondo H, Akiyama H, Ikeda K (1995) Single-laser three-color immunolabeling of a histological section by laser scanning microscopy: application to senile-plaque related structures in postmortem human brain tissue. J Histochem Cytochem 43:103–106

Uchihara T, Nakamura A, Nagaoka U, Yamazaki M, Mori O (2000) Dual enhancement of double immunofluorescent signals by CARD: participation of ubiquitin during formation of neurofibrillary tangles. Histochem Cell Biol 114:447–451

Van der Loos CM, Das PK, Van den Oord JJ, Houthoff HJ (1989) Multiple immunoenzyme staining techniques. Use of fluoresceinated, biotinylated and unlabelled monoclonal antibodies. J Immunol Methods 117:45–52

Verkkoniemi A, Kalimo H, Paetau A, Somer M, Iwatsubo T, Hardy J, Haltia M (2001) Variant Alzheimer disease with spastic paraparesis: neuropathological phenotype. J Neuropathol Exp Neurol 60:483–492

Summary of Clinical Data

Case No. (n)	Age, y*	Sex	Time**	Ischemic Lesion***	Diagnosis
1	93	F	8 d	Lt F	Infarction
2	69	M	8 d	Rt MCA	Infarction
3	89	F	11 d	Rt P, O	Infarction
4	68	F	13 d	Lt F, P	Infarction
5	66	F	14 d	Rt F	Infarction
6†	85	F	4.5 m	Rt MCA	Infarction
7†	66	M	5 m	Rt F	Infarction
8	49	M	7 m	Rt F, P	Infarction
9	77	F	10 m	Rt F, P, O	Infarction
10–15 (6)	66–84	2M/4F	4–16 y	F/T	AD
16–23 (8)	53–90	5M/3F		F/T	Normal

*Age at death; **time from onset of ischemic attack or Alzheimer disease (AD) to death; ***major focus of ischemia corresponding to the fatal ischemic attack; †cases used for Western blot analysis.

Lt indicates left; F, frontal lobe; Rt, right; MCA, middle cerebral artery; P, parietal lobe; O, occipital lobe.

Cellular localization of ApoE epitope was examined on double-labeled sections with the following combinations of probes: anti-carbindin[21] (1:3000; anti-spot 35, rabbit polyclonal antibody; generous gift from Dr Yamakuni, Tohoku University) as a marker for neurons/ApoEAB947; anti–glial fibrillary acidic protein (1:1000; mouse monoclonal antibody; DAKO) as a marker for astrocytes/ApoEC; or biotinylated *Ricinus communis* agglutinin (1:1000; RCA-120; Seikagakukougyou) as a marker for microglia/ApoEC. After one of the probes (antibody or lectin) was visualized with diaminobenzidine and nickel ammonium sulfate as purple, the sections were subjected to second-cycle immunostaining with the other probe. They were then treated similarly except that diaminobenzidine was used without nickel ammonium sulfate to yield brown reaction products.

To localize ApoE-like immunoreactivity in relation to axons, double immunolabeling with ApoEC and anti-neurofilament (SMI31; Sternberger Monoclonal) was performed. Deparaffinized sections were incubated with SMI31 (1:1000), and the epitope was then immunofluorolabeled by FITC-conjugated anti-mouse IgG (1:200; Cappel). The FITC signal was observed under the fluorescence microscope combined with a laser confocal system (TCS-SP; Leica), and the images were captured and recorded on magneto-optical disks. The same section was subjected to second-cycle immunostaining with ApoEC (1:2000), visualized with the ABC method. The already photographed axons were identified with the use of various structures such as lipofuscin granules or blood vessels as landmarks. The relationship between ApoE-like immunoreactivity and neurofilaments was assessed on the same field.

Cell Culture, Cell Stimulation, and Protein Extraction

The human neuroblastoma cell line GOTO[22] was cultured in RPMI 1640 medium supplemented with 20% fetal bovine serum. At 3 days in culture, the incubation medium was replaced with RPMI 1640 without fetal bovine serum. Hydrogen peroxide was added directly to the medium to produce a final concentration of 0.2 mmol/L and incubated for appropriate times. At fixed intervals (4, 24, and 48 hours) after the challenge with hydrogen peroxide, the incubation medium was rapidly aspirated, and the cells were washed twice with ice-cold PBS and fixed by 10% trichloroacetic acid for 30 minutes at 4°C. After the dishes were scraped with a rubber policeman, the lysate was centrifuged at 15 000*g* for 5 minutes, and the supernatant was discarded. Then each pellet of GOTO cell, at different intervals after the exposure to hydrogen peroxide, was resuspended by sonication in a sample buffer containing 9 mol/L urea, 2% Triton X, and 5% 2-mercaptoethanol. Then one fifth volume of 10% lithium dodecyl sulfate solution and approximately 2 μL of 1 mol/L Tris solution were added to the sample buffer, and the samples were sonicated again.

Each human brain homogenate from the autopsied brains (2 AD brains, 2 brains with infarction, and 4 control brains) was also fixed by 10% trichloroacetic acid, and extracted protein was treated in the same way as the GOTO cell.

Western Blot Analyses

Lysates containing equal amounts of protein (GOTO, 10 μg; autopsy brains, 10 μg) were subjected to 10% sodium dodecyl sulfate–polyacrylamide gel electrophoresis. Proteins were then transferred to a polyvinylidene difluoride membrane. The blots were blocked with 10% (wt/vol) skim milk and 0.1% Tween 20 in Tris-buffered saline (TBS) at room temperature for 1 hour and washed in 1% (wt/vol) bovine serum albumin/TBS at room temperature for 10 minutes. Then the blots were probed with ApoEC (1:4000) or ApoEAB947 (1:4000) in 1% bovine serum albumin/TBS solution at 4°C for 3 days. After 3 washes with 1% (wt/vol) skim milk and 0.1% Tween 20 in TBS at room temperature for 30 minutes, the blots were incubated with horseradish peroxidase–coupled goat anti-rabbit IgG secondary antibody (Pierce) diluted to 1:2000 with 1% skim milk/TBS at room temperature for 2 hours. Then the blots were washed 3 times with 0.1% Tween 20/TBS and visualized with the use of an enhanced chemiluminescence system (Amersham). The same blots were reprobed with anti–β-actin (1:40 000; Sigma) and visualized with horseradish peroxidase–coupled anti-mouse IgG secondary antibody (Kirkegaard and Perry Laboratory Inc). ApoE-immunoreactive bands were digitally captured, and their relative intensities were quantified with NIH Image (version 1.62). Because the number of the samples was not very large, quantified data were analyzed not only with ANOVA and the Fisher protected least significant difference test but also with the nonparametric rank method of Kruskal-Wallis.

Results

Immunolocalization of ApoE in Human Brains

Neurons exhibited an intense ApoE-like immunoreactivity at the periphery of ischemic focus (Figure 1A). This ApoE-like immunoreactivity was completely abolished throughout the adjacent section when ApoEC was coincubated with the antigen peptide (Figure 1B, the same area as Figure 1A), which confirmed the specificity of ApoE-like immunoreactivity with ApoEC. ApoEAB947 gave essentially the same